METTL3 inhibits LINC00312 to suppress osteoporosis progression in a YTHDF2-dependent manner

YANG WANG[1], YIHAO TIAN[2*] and GANG YAO[3*]

[1]Department of Ultrasound, Shengjing Hospital, China Medical University, Shenyang, Liaoning 110004, P.R. China; [2]Department of Pathology, General Hospital of Northern Theater Command, Beifang Hospital of China Medical University, Shenyang, Liaoning 110004, P.R. China; [3]Department of Orthopedic Surgery, Shengjing Hospital, China Medical University, Shenyang, Liaoning 110004, P.R. China

Received June 17, 2025; Accepted October 24, 2025

DOI: 10.3892/ijmm.2025.5699

Abstract. The regulation of methylation and non-coding RNAs plays important roles in the pathogenesis of osteoporosis. Most microRNAs (miRNAs or miRs) exert their biological functions through target genes. Long non-coding RNAs function as competing endogenous RNAs. hFOB 1.19 cells were transfected with miR-4765, LINC00312 and METTL3-related molecules. LINC00312 and miR-4765 expression was detected by PCR, whereas cleaved caspase 3 and FOXK2/SFRP1 levels were detected by western blotting. Micro-computed tomography was used to detect the bone microstructure. Diabetic mice received treatments targeting METTL3 and LINC00312. FOXK2/SFRP1 expression was detected using PCR and immunohistochemistry. The results showed that miR-4765 overexpression reduced FOXK2/SFRP1 and cleaved caspase 3 expression, causing cell apoptosis. LINC00312 inhibition was observed both *in vitro* and *in vivo*. LINC00312 binds directly to miR-4765, whereas miR-4765 binds directly to FOXK2/SFRP1. METTL3 and YTHDF2 directly bind LINC00312 and reduce its expression by altering its methylation levels. In conclusion, LINC00312 promotes the apoptosis of hFOB 1.19 cells by targeting the miR-4765/FOXK2/SFRP1 axis, and METTL3 regulates LINC00312 expression in a YTHDF2-dependent manner.

Correspondence to: Dr Yihao Tian, Department of Pathology, General Hospital of Northern Theater Command, Beifang Hospital of China Medical University, 83 Wenhua Road, Shenhe, Shenyang, Liaoning 110004, P.R. China
E-mail: 18940121470@163.com

Dr Gang Yao, Department of Orthopedic Surgery, Shengjing Hospital, China Medical University, 36 Sanhao Street, Heping, Shenyang, Liaoning 110004, P.R. China
E-mail: yaogang@cmu.edu.cn

*Contributed equally

Abbreviations: OP, osteoporosis; lncRNA, long non-coding RNA; ceRNA, competing endogenous RNA; micro-CT, micro-computed tomography; IHC, immunohistochemistry; m6A, N6-methyladenosine; miRNAs, microRNAs; CCK-8, Cell Counting Kit-8; NC, negative control; OD, optical density; RT-qPCR, reverse transcription-quantitative PCR; RIPA, radioimmunoprecipitation assay; PVDF, polyvinylidene difluoride; RIP-qPCR, RNA immunoprecipitation-qPCR; STZ, streptozotocin; FINS, fasting plasma insulin; OE, overexpression; PBS, phosphate-buffered saline; UTR, untranslated region; miRDB, microRNA database; DIANA, DNA intelligent analysis; U2OS, human osteosarcoma cell line; BMSCs, bone marrow stromal/mesenchymal stem/stromal cells

Key words: LINC00312, ceRNA, bioinformatic analysis, methylation, osteoporosis

Introduction

Osteoporosis (OP) is a metabolic disease that can be categorized as primary or secondary (1). With the annual increase in the incidence of OP, related research has intensified in recent years (2). However, the specific pathogenic mechanisms underlying OP remain unclear (3). Current evidence suggests that excessive apoptosis of osteoblasts is one of the causes of OP (4,5). Osteoblast apoptosis occurs as a result of hyperglycemia (6,7), estrogen deficiency (8,9), long-term metabolic disorders (10) and glucocorticoid abnormalities (11).

Apoptosis refers to the process of programmed cell death in multicellular organisms (12). Previous studies have revealed that inhibition of osteoblast apoptosis may improve OP prognosis (13,14). However, effective strategies for maintaining osteoblast viability and preventing cell death under hyperglycemic conditions remain uncertain (6,7).

Methylated RNA nucleotides are present in all kingdoms of life and numerous biological processes rely on dynamic and reversible methylation of coding and non-coding RNAs (15). N6-methyladenosine (m6A) RNA methylation is the most common reversible RNA modification that regulates several important RNA processes after transcription (16). Appropriate RNA methylation is crucial for cell development and tissue homeostasis (17). As a reversible post-translational modification, RNA methylation also affects RNA stability (18). Among eukaryotes, m6A is the predominant type of RNA modification, accounting for 60% of all RNA modifications (19).

Microarrays are high-throughput platforms used to analyze gene expression and to examine a broad range of signaling pathways with considerable reliability (20,21). In the present

study, focus was addressed on the expression of miR-4765. Forkhead box protein K2 (FOXK2), secreted frizzled-related protein 1 (SFRP1) and LINC00312 were predicted using publicly available online databases. Finally, the methylation site of LINC00312 was predicted using SRAMP.

The results of the present study revealed that miR-4765 inhibits apoptosis by targeting FOXK2 and SFRP1, whereas LINC00312 promotes apoptosis by binding to miR-4765. Moreover, METTL3 increases the methylation of LINC00312 in a YTHDF2-dependent manner, thereby reducing LINC00312 expression.

Materials and methods

Database usage. The gene expression profile dataset GSE74209 was selected from the GEO database (https://www.ncbi.nlm.nih.gov/geo/). GSE74209 was generated using the Agilent GPL20999 platform titled miRCURY LNA microRNA Array, 7th generation (hsa, miRBase 20; https://www.mirbase.org/) and was submitted by De-Ugarte *et al* (22). The GSE74209 dataset contained 12 samples, of which six were from patients with OP and the other six were bone tissues from healthy controls. Thereafter, the GSE74209 dataset was analyzed using the GEO2R method (Fig. S1A-H). After obtaining differentially expressed microRNAs (miRNAs or miRs), enrichment analysis was performed on the upregulated and downregulated miRNAs (Fig. S2A-E). miR-4765 expression levels were detected in GSE74209 cells (Fig. S2F and Table SI). miR-4765 was selected as the target miRNA because its differential expression was the most significant. The target genes of miR-4765 were predicted by identifying overlapping genes across different databases [TargetScan, http://www.targetscan.org/; microRNA database (miRDB, http://mirdb.org/); and DNA Intelligent Analysis (DIANA; http://diana.imis.athena-innovation.gr/)]. It was observed that miR-4765 has two overlapping genes, FOXK2 and SFRP1. Bioinformatic analysis was performed on the union set of all possible target genes (Fig. S3A-D, Tables SII and SIII). Using sequence alignment (BLAST), LINC00312 was found to closely correlate with miR-4765 expression (Fig. S4A and B). Finally, using the SRAMP database (http://www.cuilab.cn/sramp), the possible methylation sites on LINC00312 were predicted.

Cell culture. hFOB 1.19, a well-characterized human osteoblastic cell line, is widely used in OP research because of its stable osteoblastic phenotype (for example, expression of osteocalcin and collagen I) and responsiveness to osteogenic stimuli. Human-derived hFOB 1.19 cells (Chinese Academy of Sciences) are commonly used as *in vitro* models of osteogenic apoptosis. hFOB 1.19 cells were propagated in DMEM/F12 (Hyclone; Cytiva) supplemented with 10% fetal bovine serum (Hyclone; Cytiva) and 1% streptomycin and penicillin (Hyclone; Cytiva), after which they were incubated at maximum humidity in a 35˚C incubator containing 5% CO_2 and 95% air. The culture medium was replaced daily. The cells were incubated in serum-free medium for 24 h before treatment and then cultured for 5 days in the presence of varying concentrations (1, 2.5, 3.5 and 4.5 g/l) of glucose at 35˚C.

Cell Counting Kit-8 (CCK-8). Processed cells were inoculated into a 96-well plate at a concentration of $5x10^3$ cells/well. After allowing the cells to adhere to the well surface, reagents were added to each well using a reagent kit of 10 μl (Dojindo Molecular Technologies, Inc.) according to the manufacturer's instructions followed by incubation in a CO_2 incubator (35˚C, 5% CO_2 and 95% air) for 1 h. Finally, enzyme-linked immunosorbent assay (ELISA) was performed (ELx808; BioTek, Inc.), and the absorbance (wavelength set at 450 nm) in each well was measured using optical density (OD) values to represent the relative number of cells.

Cell transfection. MicroRNA-4765 (miRNA-4765) mimics, miRNA-4765 inhibitors, and a nonsense sequence as the miRNA negative control (NC) were obtained from Shanghai GenePharma Co., Ltd. The LINC00312 overexpression (OE) plasmid, sh-LINC00312, and a nonsense sequence of the long non-coding RNA (lncRNA) NC were obtained from Shanghai GeneChem Co., Ltd. The METTL3 OE plasmid, YTHDF2 OE plasmid, sh-METTL3, sh-YTHDF2, and a nonsense sequence similar to NC were obtained from Shanghai GeneChem Co., Ltd. hFOB 1.19 cells were transfected with Lipofectamine 2000 containing 2 μg plasmid or 5 μl miRNA oligo (Invitrogen; Thermo Fisher Scientific, Inc.) for 6 h at 35˚C following the manufacturer's instructions. RNA was extracted 24 h after transfection and proteins were extracted 48 h after transfection.

Reverse transcription-quantitative PCR (RT-qPCR). Total RNA was extracted from the cells using the TRIzol reagent following the manufacturer's protocol (Qiagen Sciences, Inc.). Reverse transcription PCR of miRNAs, lncRNAs and mRNAs was performed using the PrimeScript RT Reagent Kit (TaKaRa Biotechnology Co., Ltd.) according to the manufacturer's instructions. RT-qPCR was performed using the QuantiTect SYBR Green PCR Kit (TaKaRa Biotechnology Co., Ltd.), and the results were analyzed using a Roche Light Cycler® 480 II system (Roche Diagnostics). First, an initial denaturation step was performed at 95˚C for 2 min. This was followed by 40 cycles of amplification, each consisting of denaturation at 95˚C for 30 sec, annealing at 55˚C for 30 sec, and extension at 72˚C for 30 sec. The relative miRNA expression of each gene was normalized to that of U6 RNA, whereas the relative mRNA and lncRNA expression of each gene was normalized to that of GAPDH RNA. Relative quantification of gene expression was performed using the $2^{-\Delta\Delta Cq}$ method. The following primer sequences were used: miR-4765 forward, 5'-CCGCGTGAGTGATTGATAGCTATGTTC-3' and reverse, 5'-GTGCAGGGTCCGAGGT-3'; U6 forward, 5'-CTCGCTTCGGCAGCACA-3' and reverse, 5'-AACGCTTCACGAATTTGCGT-3'; LINC00312 forward, 5'-AGGGCAGGGTACTCTGATTGGC-3' and reverse, 5'-TGGCTTCTCTCCTGGCTCTGC-3'; FOXK2 forward, 5'-AAGAACGGGGTATTCGTGGAC-3' and reverse, 5'-CTCGGGAACCTGAATGTGC-3'; SFRP1 forward, 5'-ACGTGGGCTACAAGAAGATGG-3' and reverse, 5'-CAGCGACACGGGTAGATGG-3'; METTL3 forward, 5'-TTGTCTCCAACCTTCCGTAGT-3' and reverse, 5'-CCAGATCAGAGAGGTGGTGTAG-3'; YTHDF2 forward, 5'-AGCCCCACTTCC

TACCAGATG-3' and reverse, 5'-TGAGAACTGTTATTT CCCCATGC-3'; and GAPDH forward, 5'-GGAGCGAGA TCCCTCCAAAAT-3' and reverse, 5'-GGCTGTTGTCAT ACTTCTCATGG-3'. The following short hairpin (shRNA) target sequences (excluding plasmid backbone sequences) were employed in the present study: Mimics, sense 5'-UGA UUGAUAGCUAUGUUCAA-3' and antisense 5'-UUGAAC AUAGCUAUCAAUCA-3'; Mimics-NC sense, 5'-UUCUCC GAACGUGUCACGUTT-3' and antisense, 5'-ACGUGA CACGUUCGGAGAATT-3'; Inhibitor, 5'-UUGAACAUA GCUAUCAAUCA-3' and Inhibitor-NC, 5'-CAGUACUUU UGUGUAGUACAA-3'. Additionally, the following shRNA constructs were used: Sh-FOXK2, CCGAGTGATGCCATC TGACCTCAAT; Sh-SFRP1, GAGTACGACTACGTGAGC TTCCAGT; Sh-LINC00312, CCGCTTGCTGATGGACTC CAAGTAT; Sh-METTL3, GGAGGAGTGCATGAAAGC CAGTGAT; Sh-YTHDF2, AGTCCCTCCATTGGCTTC TCCTATT; and Sh-NC, 5'-CCUAAGGUUAAGUCGCCC UCG-3'.

Western blotting. hFOB 1.19 cells were lysed in radioimmunoprecipitation assay (RIPA) buffer (Beyotime Institute of Biotechnology) containing the protease inhibitor phenyl-methyl-sulfonyl fluoride (Beyotime Institute of Biotechnology), followed by centrifugation of the lysates (12,000 x g) at 4˚C for 30 min. Protein concentration was determined using a Bicinchoninic Acid Protein Kit (Beyotime Institute of Biotechnology) at a concentration of 3 μg/μl in RIPA and loading buffer. Cell lysates were separated using 10% sodium dodecyl sulfate-polyacrylamide gel electrophoresis at 150 V with protein ladders (cat. no. 26616; Thermo Fisher Scientific, Inc.), after which the 30 μl proteins were transferred to polyvinylidene difluoride (PVDF) membranes at 350 mA for 90 min. Membranes were incubated in 5% bovine serum albumin (BSA; Beijing Solarbio Science & Technology Co., Ltd.) solution for 2 h at room temperature (20-25˚C) and then with the following primary antibodies at 4˚C overnight (concentrations were considered according to the manufacturer's instructions): Anti-cleaved caspase-3 (1:1,000; cat. no. 9661; Cell Signaling Technology, Inc.), anti-FOXK2 (1:1,000; cat. no. 12008; Cell Signaling Technology, Inc.), anti-SFRP1 (1:1,000; cat. no. 4690; Cell Signaling Technology, Inc.), anti-METTL3 antibody (1:1,000; cat. no. ab195352; Abcam), anti-YTHDF2 antibody (1:1,000; cat. no. ab220163; Abcam) and anti-GAPDH (1:10,000; cat. no. 10494-1-AP; Proteintech Group, Inc.). The membranes were then incubated with a secondary antibody (1:10,000; cat. no. SA00001-2; Proteintech Group, Inc.) for 2 h at room temperature (20-25˚C) and visualized using an Ultrasensitive Enhanced Chemiluminescence Detection kit (cat. no. PK10002; Proteintech Group, Inc.). ImageJ software (v1.52; National Institutes of Health) was used for densitometric analysis.

Flow cytometry assay for apoptosis. Apoptosis was quantified using an Annexin V-FITC/PI Apoptosis Detection Kit (Dojindo Laboratories, Inc.) following the manufacturer's instructions. Briefly, hFOB1.19 cells were seeded into a 6-well plate at a density of $5x10^5$ cells per well and then treated according to the experimental requirements for each group. After treatment, cells were collected, washed twice with cold phosphate-buffered saline (PBS), and resuspended in 1X Annexin V binding buffer to achieve a concentration of ~$1x10^6$ cells/ml. Subsequently, 100 μl of the cell suspension was mixed with 5 μl of Annexin V-FITC and 5 μl of PI and then incubated at room temperature (20-25˚C) in the dark for 15 min. After incubation, 400 μl of 1X Annexin V binding buffer was added to each sample. Flow cytometry was performed using a Beckman Coulter CytoFLEX flow cytometer (Beckman Coulter Inc.). Data acquisition and analysis were performed using the FlowJo version 10.8.1 software (BD Biosciences). The cells were classified as follows: Annexin V-FITC-negative/PI-negative (viable cells), Annexin V-FITC-positive/PI-negative (early apoptotic cells), Annexin V-FITC-positive/PI-positive (late apoptotic/necrotic cells), and Annexin V-FITC-negative/PI-positive (necrotic cells). The total percentage of apoptotic cells was calculated as the sum of early apoptotic (Annexin V^+/PI^-) cells and late apoptotic (Annexin V^+/PI^+) cells.

Dual-luciferase reporter experiment. 293T cells (Chinese Academy of Sciences) were seeded onto 24-well plates and cultured overnight, followed by transfection with wild- and mutant-type FOXK2 and SFRP1 plasmids (0.1 μg pMIR-REPORT-wild-type-FOXK2 and pMIR-REPORT-wild-type-SFRP1 or pMIR-REPORT-mutant-type-FOXK2 and pMIR-REPORT-mutant-type-SFRP1 plasmids per well) (Shanghai GeneChem Co., Ltd.) using Roche X-tremeGENE HP (cat. no. 06366236001; Roche Diagnostics) according to the manufacturer's instructions. The cells were then co-transfected with either 0.4 μg miR-4765 mimics or 0.4 μg miR-4765 NCs (Shanghai GenePharma Co., Ltd.). Luciferase activity was quantified 48 h after transfection using the Dual-Luciferase Reporter Assay System according to the manufacturer's instructions (Promega Corporation). Firefly luciferase activity was normalized to the *Renilla* luciferase activity.

293T cells (Chinese Academy of Sciences) were seeded into 24-well plates and cultured overnight, followed by transfection with wild- and mutant-type LINC00312 plasmids (0.1 μg pMIR-REPORT-wild-type-LINC00312 or pMIR-REPORT-mutant-type-LINC00312 plasmids per well) (Shanghai GeneChem Co., Ltd.) using Roche X-tremeGENE HP (cat. no. 06366236001; Roche Diagnostics) according to the manufacturer's instructions. The cells were then co-transfected with either 0.4 μg miR-4765 mimics or 0.4 μg miR-4765 NCs (Shanghai GenePharma Co., Ltd.). Luciferase activity was quantified 48 h after transfection using the Dual-Luciferase Reporter Assay System according to the manufacturer's instructions (Promega Corporation). Firefly luciferase activity was normalized to the *Renilla* luciferase activity.

293T cells (Chinese Academy of Sciences) were seeded onto 24-well plates and cultured overnight, following which they were transfected with wild- and mutant-type LINC00312 plasmids (0.1 μg pMIR-REPORT-wild-type-LINC00312 or pMIR-REPORT-mutant-type-LINC00312 plasmids per well) (Shanghai GeneChem Co., Ltd.) using Roche X-tremeGENE HP (cat. no. 06366236001; Roche Diagnostics) according to the manufacturer's instructions. The cells were then co-transfected with either 0.4 μg METTL3/YTHDF2 OE plasmids or 0.4 μg METTL3/YTHDF2 NCs (Shanghai GeneChem Co.,

Ltd.). Luciferase activity was quantified 48 h after transfection using the Dual-Luciferase Reporter Assay System according to the manufacturer's instructions (Promega Corporation). Firefly luciferase activity was normalized to the *Renilla* luciferase activity.

m6A quantification. EpiQuik™ m6A RNA Methylation Quantification Kit (Colorimetric, P-9005) (Epigentek Group Inc.) was used to detect m6A levels from extracted RNA according to the manufacturer's instructions. Each well contained 200 ng of RNA. Finally, an ELISA was performed (ELx808; BioTek, Inc.), and the absorbance (wavelength set at 450 nm) in each well was measured using OD values to represent the relative methylation level.

RNA immunoprecipitation-qPCR (RIP-qPCR). RIP experiments were conducted using a Magna RIP kit (cat. no. 17-700; MilliporeSigma) according to the manufacturer's instructions. For these experiments, anti-m6A (cat. no. ab151230), anti-METTL3 (EPR18810; cat. no. ab195352), anti-YTHDF2 (EPR20318; cat. no. ab220163), and IgG were used as NCs. Finally, RNA was isolated and purified from the binding proteins using proteases, and qPCR experiments were conducted using a previously described method.

Animal experiments. All animal experiments were approved by the Institutional Review Board of the General Hospital of the Northern Theater Command (approval no. 2025-26; Shenyang, China) and performed in accordance with the National Institutes of Health Guide for the Care and Use of Laboratory Animals. A total of 50 8-week-old C57BL/6J male specific-pathogen-free mice weighing 22±2 g from China Medical University were provided free access to water and food and bred under a 12/12-h light/dark cycle with the temperature set at 22.5±2.5˚C. The mice were randomly divided into the following groups: The control group (5 non-diabetic mice fed a normal diet) and the diabetic model group (45 mice fed a high-fat diet containing 60% fat, 20% protein, and 20% carbohydrates). Among the diabetic group, 20 received METTL3-related treatment, 20 received LINC00312-related treatment, and 5 remained untreated diabetic controls. The mice were intraperitoneally injected with either vehicle or streptozotocin (STZ) diluted in 0.1 M citrate buffer at a dose of 100 mg/kg. One week after STZ injection, a diabetic mouse model was considered to have been successfully established when fasting blood glucose levels reached 7.8 mmol/l and insulin sensitivity was reduced.

The experimental duration lasted 8 weeks from STZ injection to the endpoint. Humane endpoints for euthanasia included weight loss exceeding 20% of the baseline, severe lethargy, inability to eat or drink, or signs of distress (for example, hunched posture or labored breathing). Animal health and behavior were monitored daily by visual inspection and weekly body weight measurements. At study completion, all animals were euthanized under isoflurane anesthesia (5% induction, 2% maintenance), followed by cervical dislocation. Death was confirmed by the absence of a heartbeat, respiratory arrest, and fixed dilated pupils. No unexpected deaths occurred during the experiments.

Plasma measurements. Venous blood (tail vein) was collected to measure fasting blood glucose using a OneTouch glucometer analyzer (Roach Blood Glucose Instrument) and fasting plasma insulin (FINS) using a mouse insulin kit (Merck KGaA). The insulin sensitivity index was calculated as ln (FINS • FPG).

Adenovirus injection. METTL3- and LINC00312-carrying adenoviruses for OE (OE-METTL3 and OE-LINC00312), small hairpin adenoviruses (sh-METTL3 and sh-LINC00312), and the corresponding empty vector-carrying adenoviruses (OE-NC or sh-NC) were constructed by Shanghai GeneChem Co., Ltd. Thereafter, 40 successfully established diabetes mouse models were randomly selected to receive adenovirus treatment (20 received METTL3-related treatment and the remaining 20 received LINC00312-related treatment). Adenovirus-packaged OE-METTL3 and OE-LINC00312, sh-METTL3 and sh-LINC00312, or the corresponding NC was consecutively injected into the tail vein of the mice (100 μg/kg body weight) twice a week for 4 weeks. Thereafter, mouse femurs were dissected for subsequent experimental studies.

Immunohistochemistry (IHC). The femurs of the experimental mice were separated and fixed in 4% paraformaldehyde for 24 h at room temperature (20-25˚C). After fixation, the samples were decalcified in 10% ethylenediaminetetraacetic acid for 2 weeks, dehydrated, and embedded in paraffin. Finally, 3 μm-thick tissue sections were created and deparaffinized in xylene. After rehydration, sections were exposed to an antigen epitope. Peroxidase activity was quenched for 10 min with 3% H_2O_2. After washing with PBS, the sections were incubated for 30 min in 5% BSA at room temperature (20-25˚C) and then incubated overnight in primary rabbit polyclonal anti-FOXK2 (cat. no. 30660-1-AP; Proteintech Group, Inc.) and anti-SFRP1 antibody (cat. no. 26460-1-AP; Proteintech Group, Inc.) at 4˚C overnight. Next, secondary goat anti-rabbit antibody was added for 90 min at room temperature (20-25˚C). Finally, sections were processed with an ABC working solution (OriGene Technologies, Inc.) for 20 min at room temperature (20-25˚C) and developed with 3,3-diaminobenzidine (OriGene Technologies, Inc.). Brown particles were presented as positively expressed. The results were analyzed using a light microscope (Leica Microsystems GmbH).

Micro-computed tomography (micro-CT) scan. To measure the bone microstructure, the femurs and tibias of the experimental mice were separated, after which the soft tissue was removed and incubated in sterile PBS. Finally, the prepared bone tissue was placed into the micro-CT system (NEMO Micro-CT, NMC-200; Heping Medical Technology) operated according to the manufacturer's instructions (tube voltage, 80 KV; tube current, 0.06 mA; source to detector distance, 410 mm; distance from source to scanned object, 90 mm; frames per second, 20/sec; frames in all, 4,000; reconstruction type, FDK; horizontal FOV, 50 mm; axis FOV, 16 mm; pixel size 0.05x0.05x0.05 mm; scanning accuracy, 35 μm; dimensions, 1,000x1,000x608; CT threshold, 1,497.95).

Statistical analysis. All data were analyzed using IBM SPSS Statistics (version 23.0; IBM Corp.) and GraphPad Prism (version 5.0; GraphPad Software Inc.; Dotmatics). $P<0.05$ was

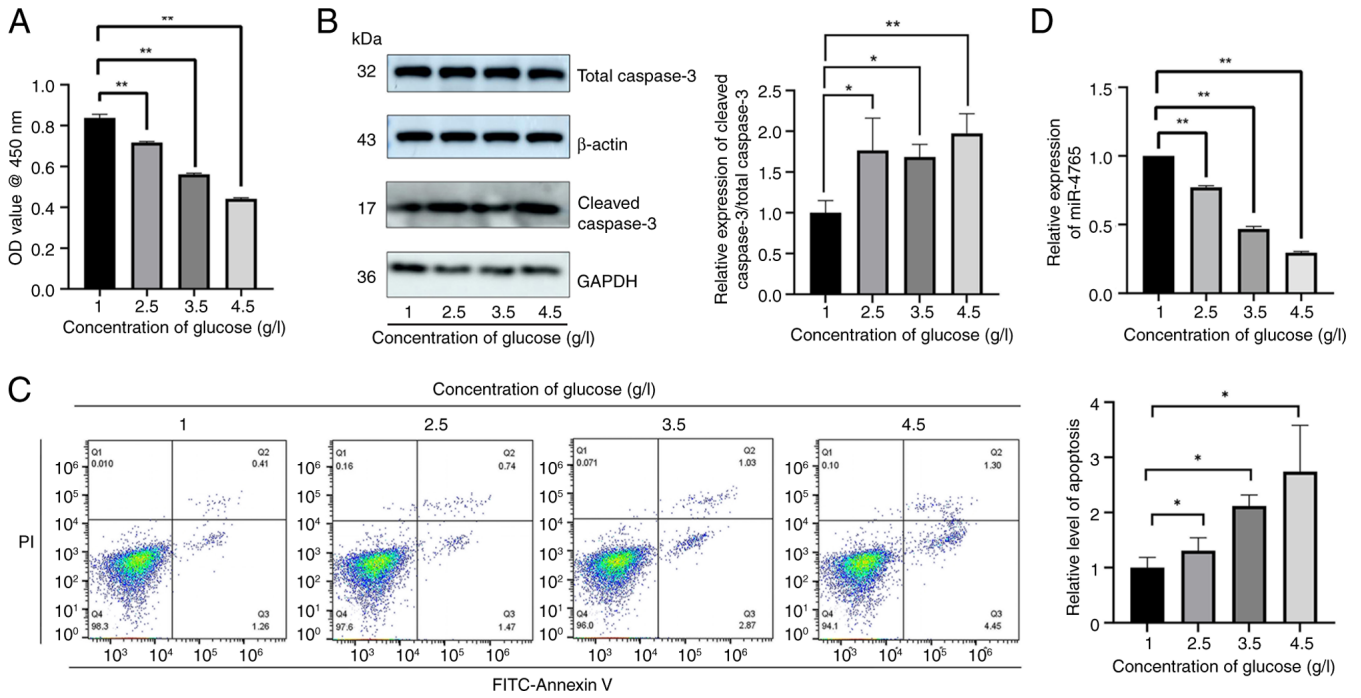

Figure 1. Hyperglycemia can induce hFOB 1.19 cell apoptosis and inhibit miR-4765 expression. (A) Viability of hFOB 1.19 cells under various glucose concentrations (1, 2.5, 3.5 or 4.5 g/l). Cell viability was expressed as OD values. (B) Cleaved caspase-3 protein expression in hFOB 1.19 cells under various glucose concentrations (1, 2.5, 3.5 or 4.5 g/l). (C) Apoptosis levels detected using Annexin V staining in hFOB 1.19 cells under various glucose concentrations (1, 2.5, 3.5 or 4.5 g/l). (D) miR-4765 expression in hFOB 1.19 cells under various glucose concentrations (1, 2.5, 3.5 or 4.5 g/l). Data are presented as the mean ± standard deviation (n=3). *P<0.05 and **P<0.01. OD, optical density; miR, microRNA.

considered to indicate a statistically significant difference. Each assay was repeated independently three times, and measurement data were expressed as the mean ± standard deviation. All pairwise comparisons were reanalyzed using Tukey's honest significant difference test. Specifically, after performing one-way ANOVA for comparisons between three or more groups, Tukey's HSD test was used to determine significant differences.

Results

Hyperglycemia induces hFOB 1.19 cell apoptosis and inhibits miR-4765 expression. To determine whether a hyperglycemic environment can cause OP, induce hFOB 1.19 cell apoptosis, and inhibit miR-4765 expression, hFOB 1.19 cells were cultured in media with various glucose concentrations (1, 2.5, 3.5, and 4.5 g/l). The results of the CCK-8 assay indicated that the number of cells decreased as the glucose concentration increased (Fig. 1A). Thereafter, western blotting was used to determine the expression level of cleaved caspase-3 (Fig. 1B); Annexin V staining was used to determine the apoptosis level (Fig. 1C); and RT-qPCR was used to determine the expression level of miR-4765 (Fig. 1D). The apoptotic level of hFOB 1.19 cells was significantly increased, whereas the expression level of miR-4765 was the lowest at a glucose concentration of 4.5 g/l. Therefore, a medium with a glucose concentration of 4.5 g/l was selected to simulate OP in the subsequent experiments.

miR-4765 inhibits hFOB 1.19 cell apoptosis. To examine the effects of miR-4765 on hFOB 1.19 cells, cells were transfected with miR-4765 mimics and miR-4765 mimic NC and subsequent experiments were conducted (Fig. 2A). The results of the CCK-8 assay showed that miR-4765 OE promoted an increase in cell count (Fig. 2B). Western blotting and Annexin V staining showed that transient transfection of miR-4765 mimics into hFOB 1.19 cells inhibited apoptosis (Fig. 2C and D). Transfection with miR-4765 inhibitors increased apoptosis (Fig. 2B-D).

FOXK2 and SFRP1 are potential target genes of miR-4765 predicted using the miRDB. To further investigate the molecular mechanisms through which miR-4765 affects apoptosis, several online target-prediction tools were used, including miRDB, DIANA and TargetScan, based on which two candidate target genes were identified (Fig. 3A). To assess the effects of miR-4765 on FOXK2 and SFRP1 expression, hFOB 1.19 cells were transfected with miR-4765 mimics and inhibitors. Accordingly, miR-4765 mimics lowered FOXK2 and SFRP1 levels, whereas miR-4765 inhibitors elevated them (Fig. 3B-D). To examine the effects of FOXK2 and SFRP1 on hFOB 1.19 cells, the cells were transfected with sh-FOXK2, sh-SFRP1, sh-FOXK2 NC, or sh-SFRP1 NC (Fig. 3E). The results of the CCK-8 assay and analysis of cleaved caspase-3 protein expression showed that FOXK2 and SFRP1 knockouts increased the number of cells (Fig. 3F-I). Moreover, transfection with FOXK2 and SFRP1 OE plasmid promoted apoptosis (Fig. 3E-I).

A hyperglycemic environment promoted the expression of FOXK2 and SFRP1 both *in vitro* and *in vivo* (Fig. 3J-L). Finally, the bone microstructure indices were assessed using micro-CT (Fig. 3M). The bone microstructure showed more features of OP in diabetic mice than in control mice.

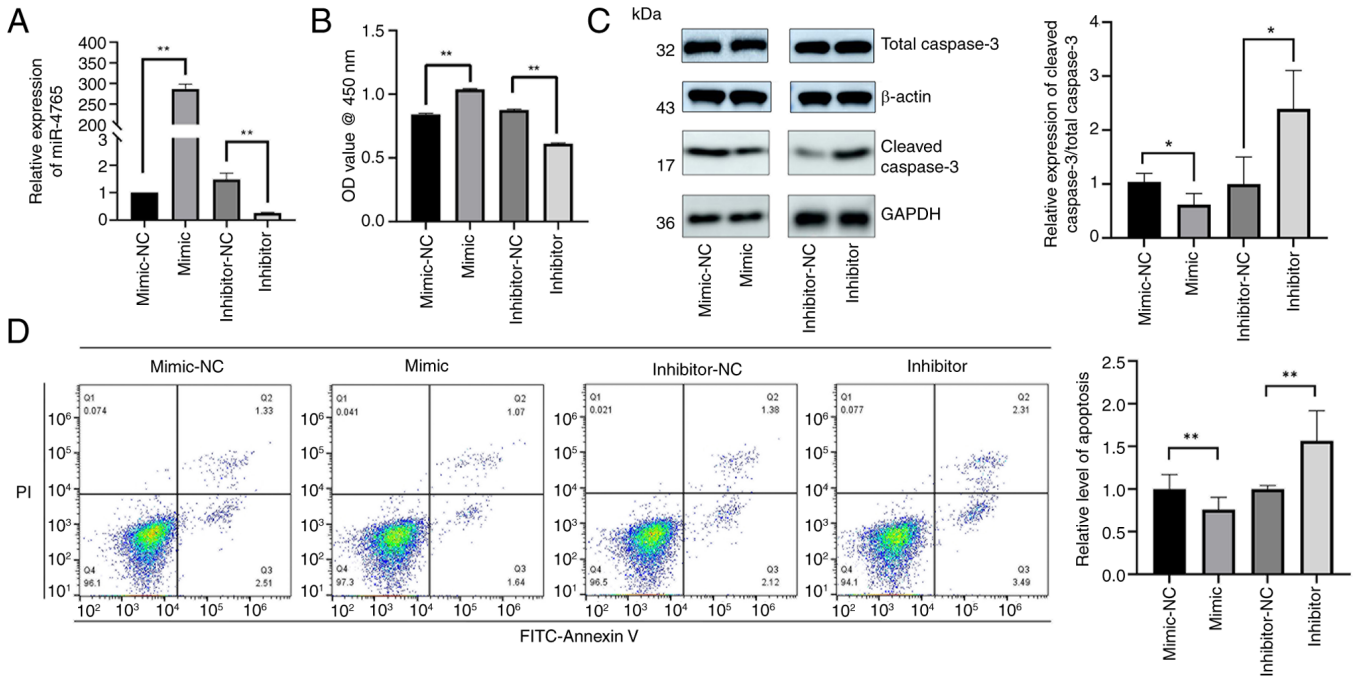

Figure 2. miR-4765 can inhibit hFOB 1.19 cell apoptosis. (A) Transfection efficiency of miR-4765 mimics and inhibitors. (B) Viability of hFOB 1.19 cells after transfection with miR-4765 mimics, inhibitors, and the corresponding NCs. Cell viability was expressed as OD values. (C) Cleaved caspase-3 protein expression after transfection with miR-4765 mimics, inhibitors, and the corresponding NCs. (D) Apoptosis levels detected using Annexin V staining after transfection with miR-4765 mimics, inhibitors, and corresponding NCs. Data are presented as the mean ± standard deviation (n=3). *P<0.05 and **P<0.01. miR, microRNA; OD, optical density; NC, negative control.

miR-4765 directly targets the 3'-untranslated region (UTR) of FOXK2 and SFRP1. The wild-type 3'-UTR of FOXK2 and SFRP1 mRNA was cloned with the predicted miR-4765 binding sites, along with the mutant-type 3'-UTR located upstream of the luciferase-coding sequence (Fig. 4A). Luciferase activity was lower in cells co-transfected with miR-4765 mimics and FOXK2/SFRP1 mRNA wild-type 3'-UTR fragments than in those co-transfected with miR-4765 mimics NC and FOXK2/SFRP1 mRNA wild-type 3'-UTR fragments. Conversely, luciferase activity was greater in cells co-transfected with miR-4765 mimics and FOXK2/SFRP1 mRNA mutant-type 3'-UTR fragments than in those co-transfected with miR-4765 mimics and FOXK2/SFRP1 mRNA wild-type 3'-UTR fragments (Fig. 4B and C). Finally, FOXK2/SFRP1 OE plasmids and miR-4765 mimics were co-transfected into hFOB 1.19 cells, and the extent of apoptosis was determined using the CCK-8 assay and cleaved caspase-3 protein expression. The results revealed that FOXK2 and SFRP1 partially reversed the anti-apoptotic effects of miR-4765 (Fig. 4D-G). These results indicated that FOXK2 and SFRP1 may be direct targets of miR-4765, suggesting that miR-4765 influences apoptosis by targeting FOXK2 and SFRP1.

LINC00312 may act as a miR-4765 sponge to regulate FOXK2 and SFRP1, as predicted using database analysis. To examine whether LINC00312 interacts with miR-4765, hFOB 1.19 cells were transfected with LINC00312 OE plasmid, sh-LINC00312, or LINC00312 NC. After confirming successful transfection (Fig. 5A), it was found that LINC00312 OE plasmids reduced miR-4765 expression, whereas sh-LINC00312 increased it (Fig. 5B).

To assess the effects of LINC00312 on FOXK2 and SFRP1, hFOB 1.19 cells were transfected with LINC00312 OE plasmid, sh-LINC00312, or LINC00312 NC. The LINC00312 OE plasmid increased FOXK2 and SFRP1 levels, whereas sh-LINC00312 decreased these levels (Fig. 5C).

To assess the effects of LINC00312 on FOXK2 and SFRP1 *in vivo*, diabetic OP mice were injected with LINC00312-carrying adenoviruses for OE-LINC00312, sh-LINC00312, or the corresponding NC. OE-LINC00312 increased the FOXK2 and SFRP1 mRNA (Fig. 5D) and protein (Fig. 5E) levels *in vivo*, whereas sh-LINC00312 decreased these levels.

LINC00312 can be directly combined with miR-4765. The wild-type 3'-region of LINC00312 was cloned with the presumed miR-4765-binding sites, along with the mutant 3'-region located upstream of the luciferase-coding sequence (Fig. 6A). Luciferase activity was lower in cells co-transfected with miR-4765 mimics and LINC00312 wild-type 3'-region fragments than in cells co-transfected with miR-4765 mimics NC and LINC00312 wild-type 3'-region fragments. Conversely, luciferase activity was greater in cells co-transfected with miR-4765 mimics and LINC00312 mutant-type 3'-region fragments than in cells co-transfected with miR-4765 mimics and LINC00312 wild-type 3'-region fragments (Fig. 6B). Finally, hFOB 1.19 cells were co-transfected with the LINC00152 OE plasmid and miR-4765 mimics, after which the extent of cell apoptosis was determined using the CCK-8 assay and cleaved caspase-3 protein expression. The results demonstrated that miR-4765 partially reversed the apoptotic effects of LINC00312 (Fig. 6C and D). Concurrently, hFOB 1.19 cells were co-transfected with the

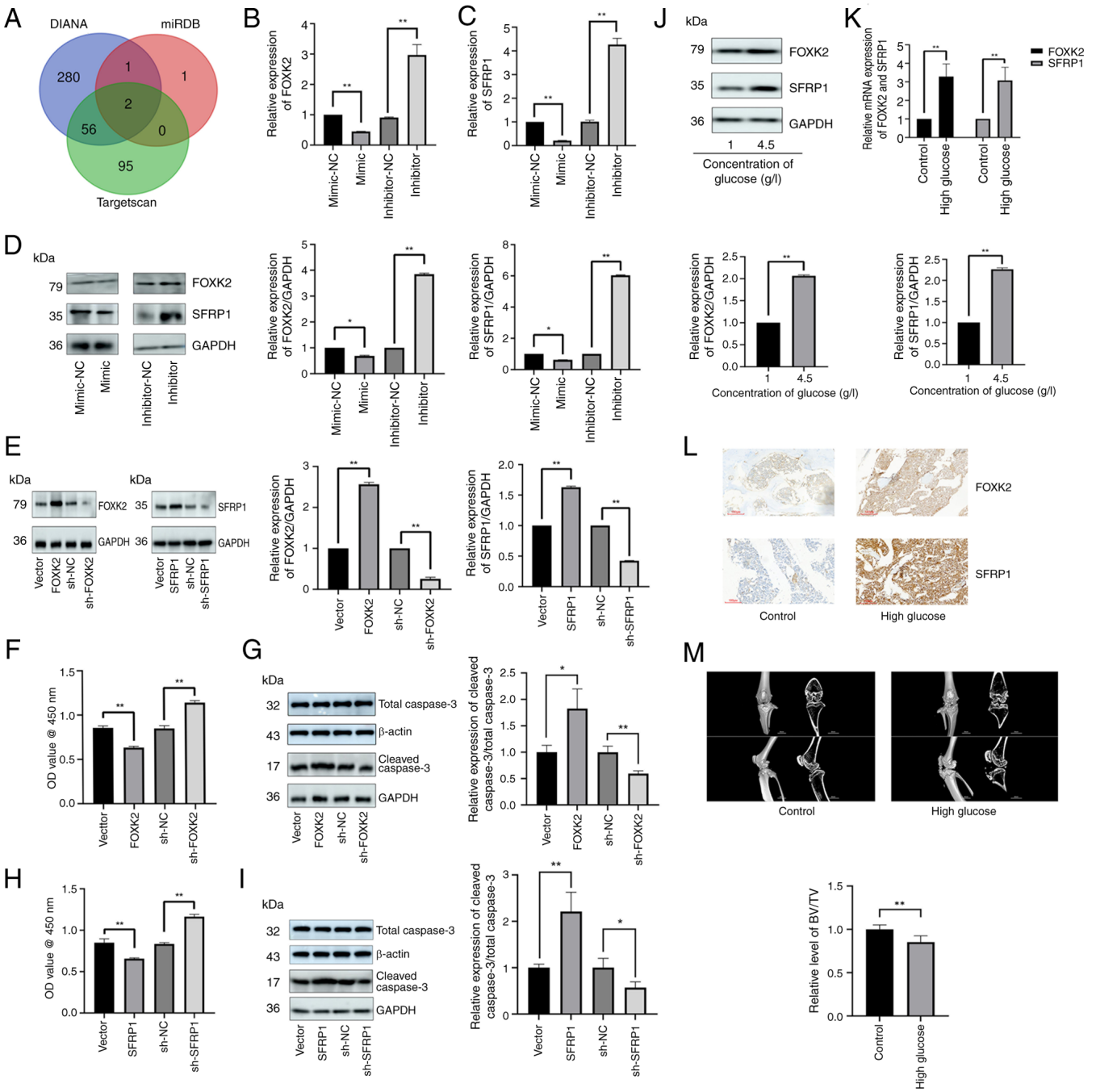

Figure 3. FOXK2 and SFRP1 are potential target genes of miR-4765 predicted using databases. (A) Venn diagram of target genes overlapping with miR-4765 from three different databases (TargetScan, miRDB and DIANA). (B) FOXK2 mRNA expression after transfection with miR-4765 mimics, inhibitors, and the corresponding NCs. (C) SFRP1 mRNA expression after transfection with miR-4765 mimics, inhibitors, and the corresponding NCs. (D) FOXK2 and SFRP1 protein expression after transfection with miR-4765 mimics, inhibitors, and corresponding NCs. (E) Transfection efficiency of FOXK2 and SFRP1 OE plasmids, sh-FOXK2 and sh-SFRP1, and the corresponding NCs. (F) Viability of hFOB 1.19 cells after transfection with FOXK2 OE plasmid, sh-FOXK2, and the corresponding NCs. Cell viability was expressed as OD values. (G) Cleaved caspase-3 protein expression after transfection with FOXK2 OE plasmid, sh-FOXK2, and the corresponding NCs. (H) Viability of hFOB 1.19 cells after transfection with SFRP1 OE plasmid, sh-SFRP1, and the corresponding NCs. Cell viability was expressed as OD values. (I) Cleaved caspase-3 protein expression after transfection with SFRP1 OE plasmid, sh-SFRP1, and the corresponding NCs. (J) FOXK2 and SFRP1 expression in hFOB 1.19 cells under various glucose concentrations (1 or 4.5 g/l). (K) FOXK2 and SFRP1 mRNA expression in the bone tissues of control and diabetic mice. (L) FOXK2 and SFRP1 protein expression determined via immunohistochemical staining in the bone tissues of control and diabetic mice with OP. (M) Micro-computed tomography of the knee joint in control and diabetic mice with OP. Data are presented as the mean ± SD (n=3). *P<0.05 and **P<0.01. miR, microRNA; NC, negative control; sh-, short hairpin; OD, optical density; OE, overexpression; OP, osteoporosis.

LINC00152 OE plasmid and sh-FOXK2 and sh-SFRP1, after which the extent of cell apoptosis was determined using the CCK-8 assay and cleaved caspase-3 protein expression. Notably, it was found that sh-FOXK2 and sh-SFRP1 partially reversed the apoptotic effects of LINC00312 on hFOB 1.19 cells (Fig. 6E-H). These results indicated that LINC00312 can directly bind to miR-4765 as an RNA sponge and exert its ceRNA function.

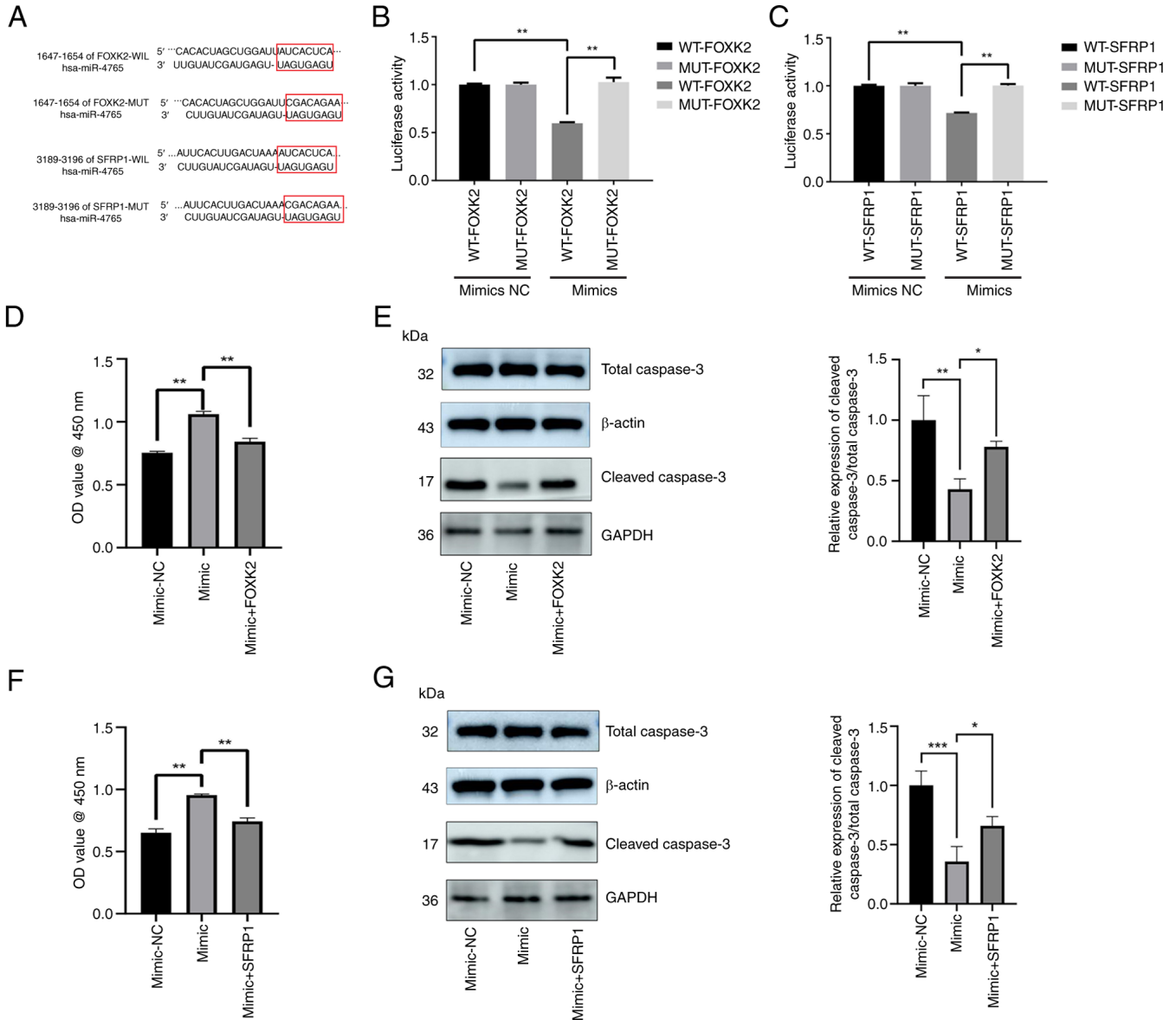

Figure 4. miR-4765 can be directly combined with the 3'-UTR of FOXK2 and SFRP1. (A) Binding sites for miR-4765 and FOXK2, miR-4765 and SFRP1. (B) Luciferase activity in 293T cells co-transfected with miR-4765 mimic and FOXK2 WT or MUT 3'-UTR. (C) Luciferase activity in 293T cells co-transfected with miR-4765 mimic and SFRP1 WT or MUT 3'-UTR. (D) Viability of hFOB 1.19 cells after co-transfection with FOXK2 OE plasmids and miR-4765 mimics and the corresponding NCs. Cell viability was expressed as OD values. (E) Cleaved caspase-3 protein expression after co-transfection with FOXK2 OE plasmids and miR-4765 mimics and the corresponding NCs. (F) Viability of hFOB 1.19 cells after co-transfection with SFRP1 OE plasmids and miR-4765 mimics and the corresponding NCs. Cell viability was expressed as OD values. (G) Cleaved caspase-3 protein expression after co-transfection with SFRP1 OE plasmids and miR-4765 mimics and the corresponding NCs. Data are presented as the mean ± standard deviation (n=3). *P<0.05, **P<0.01 and ***P<0.001. miR, microRNA; UTR, untranslated region; WT, wild type; MUT, mutant; OD, optical density; NC, negative control; OE, overexpression.

LINC00312 promotes hFOB 1.19 cell apoptosis. To examine the apoptotic effects of LINC00312 on hFOB 1.19 cells, cells were transfected with sh-LINC00312 or LINC00312 NC. The results of the CCK-8 assay demonstrated that after LINC00312 knockout increased the number of cells (Fig. 7A). Western blotting and Annexin V staining showed that transfection with sh-LINC00312 inhibited hFOB 1.19 cell apoptosis (Fig. 7B and C), whereas transfection with the LINC00312 OE plasmid increased apoptosis (Fig. 7A and B). The hyperglycemic environment promoted the expression of LINC00312 (Fig. 7D).

METTL3 reduces LINC00312 expression by increasing its methylation level. Previous studies have shown that methylation can occur in OP and that lncRNAs may undergo methylation changes. Therefore, it was proposed that changes in LINC00312 levels in OP are associated with changes in its methylation status. First, it was predicted that LINC00312 contains an m6A modification site (score=0.676) based on the SRAMP website (Fig. 8A). ELISA was used to detect differences in m6A modification levels between high glucose (HG)-induced and low glucose (LG)-cultured osteoblasts. A hyperglycemic environment inhibited methylation levels (Fig. 8B). Next, RT-qPCR and western blotting were used to detect the RNA and protein expression levels of METTL3 in osteoblasts cultured under high- and low-glucose conditions, respectively. Notably, the mRNA and protein expression levels

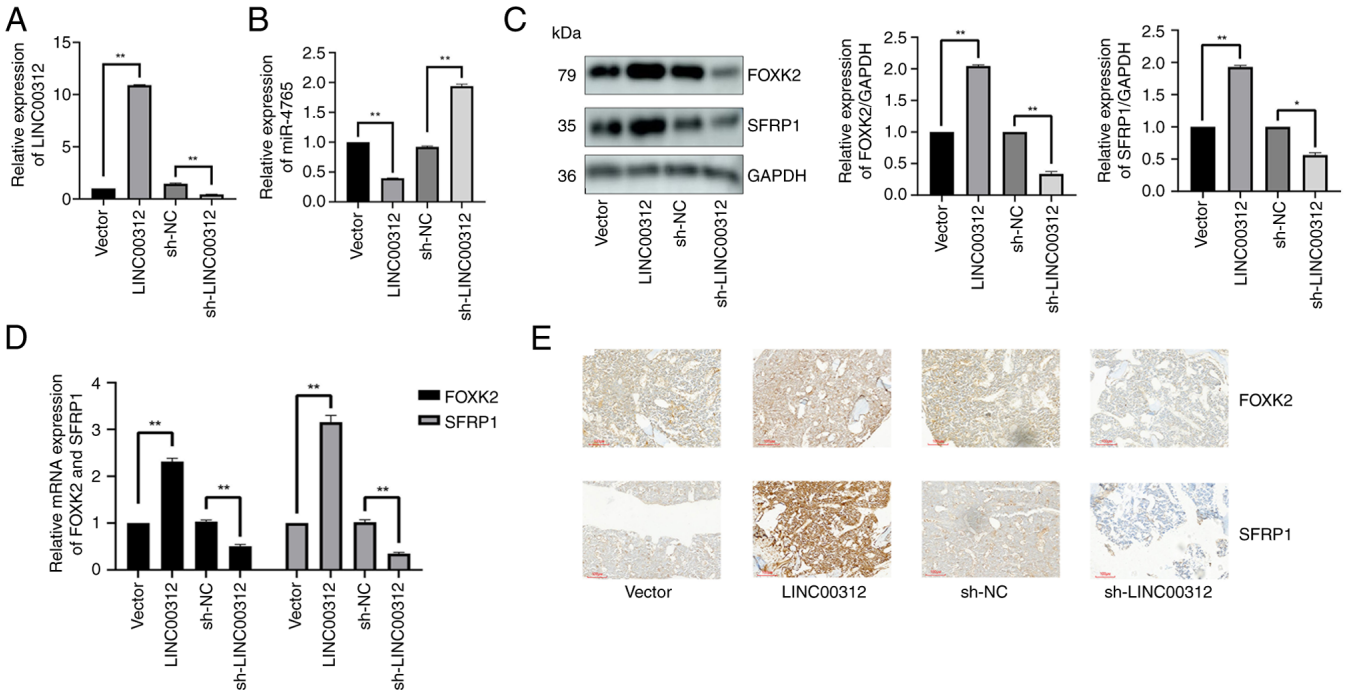

Figure 5. LINC00312 may act as an miR-4765 sponge to regulate FOXK2 and SFRP1 as predicted using the database. (A) Transfection efficiency of LINC00312 OE plasmids and sh-LINC00312. (B) miR-4765 expression after transfection with LINC00312 OE plasmids, sh-LINC00312, and the corresponding NCs. (C) FOXK2 and SFRP1 protein expression after transfection with LINC00312 OE plasmids, sh-LINC00312, and the corresponding NCs. (D) FOXK2 and SFRP1 mRNA expression in the bone tissues of diabetic mice with OP after adenovirus transfection with LINC00312 OE plasmids, sh-LINC00312, and the corresponding NCs. (E) FOXK2 and SFRP1 protein expression determined using immunohistochemical staining in the bone tissues of diabetic mice with OP after adenovirus transfection with LINC00312 OE plasmids, sh-LINC00312, and the corresponding NCs. Data are presented as the mean ± standard deviation (n=3). *P<0.05 and **P<0.01. miR, microRNA; NC, negative control; OE, overexpression; sh-, short hairpin; OP, osteoporosis.

of METTL3 decreased in the hyperglycemic environment (Fig. 8C and D).

To further investigate the biological function of METTL3, hFOB 1.19 cells were transfected with a METTL3 OE plasmid and sh-METTL3. After successful transfection (Fig. 8E and F), expression levels of the downstream LINC00312-miR-4765-FOXK2/SFRP1 axis were determined. OE of METTL3 lowered LINC00312, FOXK2, and SFRP1 expression levels, but increased miR-4765 expression levels, whereas sh-METTL3 induced the opposite effect (Fig. 8G-I). The results of the CCK-8 assay, cleaved caspase-3 protein expression, and Annexin V staining showed that METTL3 OE increased the number of cells, whereas sh-METTL3 decreased the cell number and promoted apoptosis (Fig. 8J-L). Finally, to further investigate how METTL3 inhibits LINC00312 expression, dual-luciferase reporter assay and RIP-qPCR were performed. Accordingly, it was revealed that METTL3 binds directly to LINC00312 (Fig. 8M-O). Using methylated RIP-qPCR, it was found that the m6A modification level of LINC00312 was lower in HG-induced osteoblasts than that in LG-cultured osteoblasts (Fig. 8P). Moreover, the METTL3 knockout reduced the relative enrichment of m6A in LINC00312 cells, whereas METTL3 OE had the opposite effect (Fig. 8Q).

Next, IHC was used to detect the protein expression levels of METTL3 in diabetic mice with OP and in non-diabetic mice. Notably, diabetic mice with OP exhibited decreased protein expression of METTL3 (Fig. 8R).

To assess the effects of METTL3 on FOXK2 and SFRP1 *in vivo*, diabetic mice with OP were injected with METTL3-carrying adenoviruses OE-METTL3, sh-METTL3, or the corresponding NC. Accordingly, it was found that OE-METTL3 decreased the FOXK2 and SFRP1 mRNA (Fig. 8S) and protein (Fig. 8T) expression levels *in vivo*, whereas sh-METTL3 increased them.

YTHDF2 contributes to increased LINC00312 methylation. METTL3-mediated m6A modifications typically occur in a reader-dependent manner. First, RT-qPCR and western blotting were used to detect the mRNA and protein expression levels of YTHDF2 in HG-induced and LG-cultured osteoblasts, respectively. Notably, the expression of YTHDF2 decreased in HG environments (Fig. 9A and B). To further investigate the biological function of YTHDF2, hFOB 1.19 cells were transfected with the YTHDF2 OE plasmid and sh-YTHDF2. After successful transfection (Fig. 9C and D), the expression levels of the downstream LINC00312-miR-4765-FOXK2/SFRP1 axis were determined. Notably, the YTHDF2 OE plasmid lowered LINC00312, FOXK2 and SFRP1 expression levels but increased miR-4765 expression levels, whereas sh-YTHDF2 produced the opposite effect (Fig. 9E-G). The results of the CCK-8 assay, cleaved caspase-3 protein expression, and Annexin V staining showed that YTHDF2 OE increased the number of cells, whereas sh-YTHDF2 produced the opposite effect (Fig. 9H-J). To further investigate how YTHDF2 inhibited LINC00312 expression, a dual-luciferase reporter assay was performed. Notably, it was found that YTHDF2 directly binds to LINC00312 (Fig. 9K and L). It was investigated whether METTL3 regulates m6A methylation of LINC00312

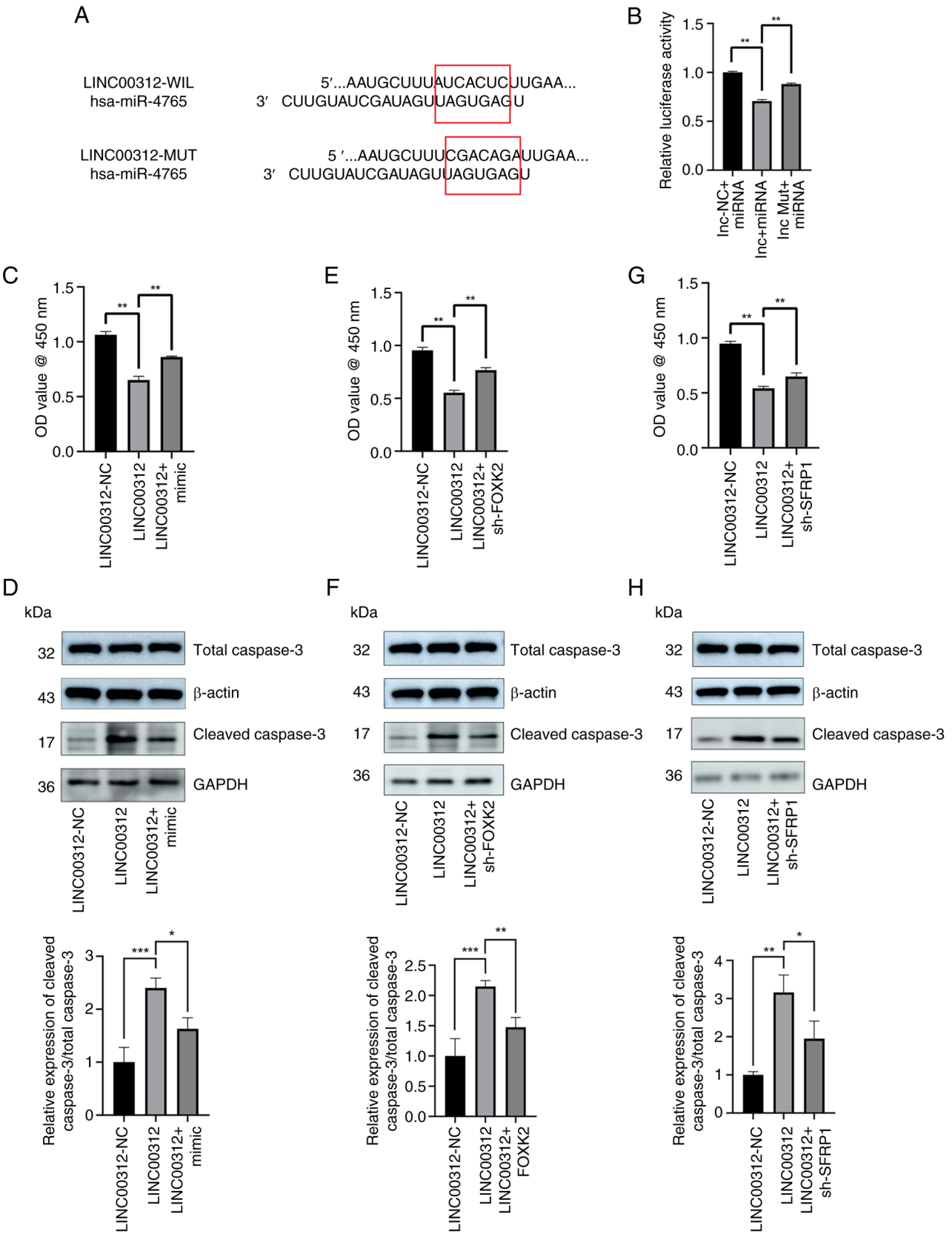

Figure 6. LINC00312 can be directly combined with miR-4765. (A) Binding sites for LINC00312 and miR-4765. (B) Luciferase activity in 293T cells co-transfected with miR-4765 mimics and LINC00312 WT or MUT 3' region. (C) Viability of hFOB 1.19 cells after co-transfection with LINC00312 OE plasmids and miR-4765 mimics and the corresponding NCs. Cell viability was expressed as OD values. (D) Cleaved caspase-3 protein expression after co-transfection with LINC00312 OE plasmids and miR-4765 mimics and the corresponding NCs. (E) Viability of hFOB 1.19 cells after co-transfection with LINC00312 OE plasmids and sh-FOXK2 and the corresponding NCs. Cell viability was expressed as OD values. (F) Cleaved caspase-3 protein expression after co-transfection with LINC00312 OE plasmids and sh-FOXK2 and the corresponding NCs. (G) Viability of hFOB 1.19 cells after co-transfection with LINC00312 OE plasmids and sh-SFRP1 and the corresponding NCs. Cell viability was expressed as OD values. (H) Cleaved caspase-3 protein expression after co-transfection with LINC00312 OE plasmids and sh-SFRP1 and the corresponding NCs. Data are presented as the mean ± standard deviation (n=3). *P<0.05, **P<0.01 and ***P<0.001. miR, microRNA; WT, wild type; MUT, mutant; OD, optical density; NC, negative control; OE, overexpression; sh-, short hairpin.

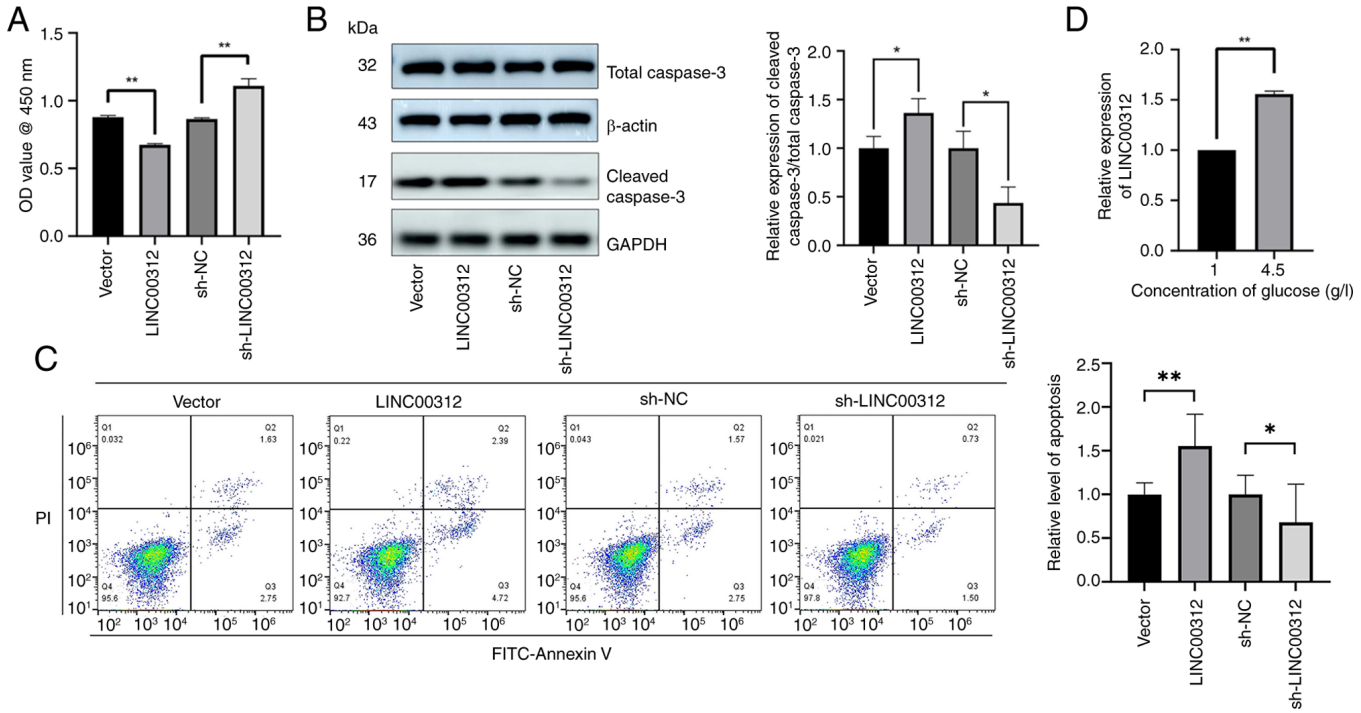

Figure 7. LINC00312 can promote hFOB 1.19 cells apoptosis. (A) Viability of hFOB 1.19 cells after transfection with LINC00312 OE plasmids, sh-LINC00312, and the corresponding NCs. Cell viability was expressed as OD values. (B) Cleaved caspase-3 protein expression after transfection with LINC00312 OE plasmids, sh-LINC00312, and the corresponding NCs. (C) Apoptosis levels determined via Annexin V staining after transfection with LINC00312 OE plasmids, sh-LINC00312, and the corresponding NCs. (D) LINC00312 expression in hFOB 1.19 cells under various glucose concentrations (1 or 4.5 g/l). Data are presented as the mean ± standard deviation (n=3). *P<0.05 and **P<0.01. OD, optical density; NC, negative control; OE, overexpression; sh-, short hairpin.

in hFOB 1.19 cells in an m6A-YTHDF2-dependent manner. RIP-qPCR was used to examine the interaction between YTHDF2 and LINC00312 after transfecting hFOB 1.19 cells with the METTL3 OE plasmid and sh-METTL3. METTL3 inhibition in hFOB 1.19 cells reduced the interaction between YTHDF2 and LINC00312 compared with that in the sh-NC group, whereas its OE had the opposite effect (Fig. 9M).

Finally, IHC was used to detect the protein expression levels of YTHDF2 in diabetic mice with OP and non-diabetic mice. Notably, the protein expression levels of YTHDF2 decreased in diabetic mice with OP (Fig. 9N).

Discussion

Based on the GSE74209 database, miR-4765 expression was increased in healthy individuals and decreased in patients with OP. Thereafter, upstream lncRNAs and downstream target genes were predicted using the databases (TargetScan, miRDB and DIANA), and LINC00312 and FOXK2/SFRP1 were identified. The m6A modification site within LINC00312 was predicted using an online database (SRAMP). Finally, cell experiments were conducted to verify the accuracy of the predictions.

FOXK2, a member of the Foxk family of forkhead transcription factors, is widely involved in various cellular activities, such as regulating aerobic glycolysis (23), suppressing the hypoxic response (24), and inhibiting atrophy and autophagy programs (25), as well as in various cell cycle regulation processes. Some studies have suggested that FOXK2 promotes apoptosis, which is consistent with the results of the present study. FOXK2 OE induces apoptosis in clear cell renal cell carcinoma cells *in vivo* (26). Moreover, another study found that FOXK2 promotes apoptosis in a human osteosarcoma cell line (U2OS) based on caspase-3 activity (27). However, other studies have suggested that FOXK2 also inhibits apoptosis. In fact, a previous study found that FOXK2 promotes granulosa cell proliferation via the PI3K/AKT/mTOR regulatory pathway (28).

SFRP1, which modulates Wnt signaling by directly interacting with Wnt, has been widely involved in various diseases, such as Alzheimer's disease (29), retinal neurogenesis (30,31) and leukemia (32), as well as in the pathogenesis of OP. Some studies have indicated that SFRP1 promotes OP, which is consistent with the results presented herein. For instance, a previous study found that increasing the expression level of SFRP1 reduced bone formation and mass (33). Another study showed that SFRP1 suppressed the proliferation of bone marrow stromal/mesenchymal stem/stromal cells (BMSCs) and decreased calcium nodule formation and alkaline phosphatase activity (34). Evidence further suggests that SFRP1, a negative regulator of the Wnt signaling pathway, is significantly upregulated in OP (35). Therefore, the inhibition of SFRP1 expression plays an important role in bone formation by inducing osteoblast differentiation (36). Nonetheless, other studies have suggested that increasing SFRP1 expression promotes bone formation and that SFRP1 can be used to treat OP (37).

LINC00312, an lncRNA, produces an intron-less transcript that is considered to function as a tumor suppressor. LINC00312 is involved in various cytological processes, such as DNA damage repair (38), invasion and migration (39-41). Moreover, LINC00312 promotes apoptosis, which is

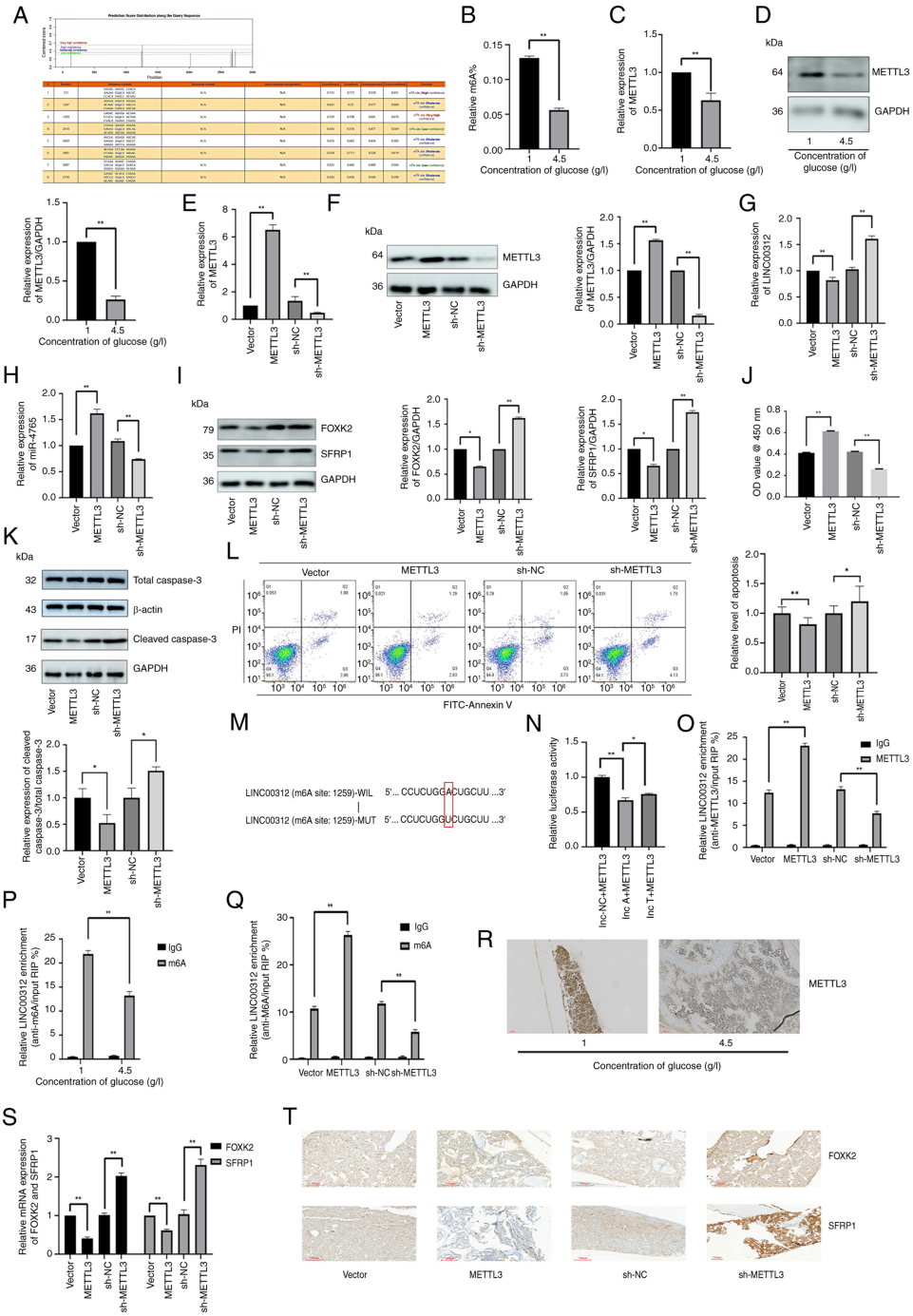

Figure 8. METTL3 reduces the expression level of LINC00312 by increasing its methylation level. (A) SRAMP was used to predict the possible m6A modification locations of LINC00312. (B) Relative m6A level of hFOB 1.19 cells under various glucose concentrations (1 or 4.5 g/l) determined via m6A colorimetric analysis. (C) METTL3 mRNA expression in hFOB 1.19 cells under various glucose concentrations (1 or 4.5 g/l). (D) METTL3 protein expression in hFOB 1.19 cells under various glucose concentrations (1 or 4.5 g/l). (E) Transfection efficiency of METTL3 OE plasmids and sh-METTL3. METTL3 mRNA expression after transfection with METTL3 OE plasmids, sh-METTL3, and the corresponding NCs. (F) Transfection efficiency of METTL3 OE plasmids and sh-METTL3; METTL3 protein expression after transfection with METTL3 OE plasmids, sh-METTL3, and the corresponding NCs. (G) LINC00312 expression after transfection with METTL3 OE plasmids, sh-METTL3, and the corresponding NCs. (H) miR-4765 expression after transfection with METTL3 OE plasmids, sh-METTL3, and the corresponding NCs. (I) FOXK2 and SFRP1 protein expression after transfection with METTL3 OE plasmids, sh-METTL3, and the corresponding NCs. (J) Viability of hFOB 1.19 cells after transfection with METTL3 OE plasmid, sh-METTL3, and the corresponding NCs. Cell viability was expressed as OD values. (K) Cleaved caspase-3 protein expression after transfection with METTL3 OE plasmids, sh-METTL3, and the corresponding NCs. (L) Apoptosis levels determined via Annexin V staining after transfection with METTL3 OE plasmids, sh-METTL3, and the corresponding NCs. (M) m6A modification locations of LINC00312. (N) Luciferase activity in 293T cells co-transfected with METTL3 OE plasmids and LINC00312 WT or MUT 3'-region. (O) Relative enrichment of METTL3 in LINC00312 after transfection with METTL3 OE plasmids, sh-METTL3, and the corresponding NCs. (P) Relative enrichment of m6A in LINC00312 under various glucose concentrations (1 or 4.5 g/l) determined via methylated RNA immunoprecipitation-quantitative PCR assays. (Q) Relative enrichment of m6A in LINC00312 after transfection with METTL3 OE plasmids, sh-METTL3, and the corresponding NCs. (R) METTL3 protein expression determined via IHC staining in the bone tissues of diabetic mice with OP and non-diabetic mice. (S) FOXK2 and SFRP1 mRNA expression in the bone tissues of diabetic mice with OP after adenovirus transfection with METTL3 OE plasmids, sh-METTL3, and the corresponding NCs. (T) FOXK2 and SFRP1 protein expression determined via IHC staining in the bone tissues of diabetic mice with OP after adenovirus transfection with METTL3 OE plasmids, sh-METTL3, and the corresponding NCs. Data are presented as the mean ± standard deviation (n=3). *P<0.05 and **P<0.01. OE, overexpression; sh-, short hairpin; WT, wild type; MUT, mutant; NC, negative control; OD, optical density; miR, microRNA; OP, osteoporosis; IHC, immunohistochemical.

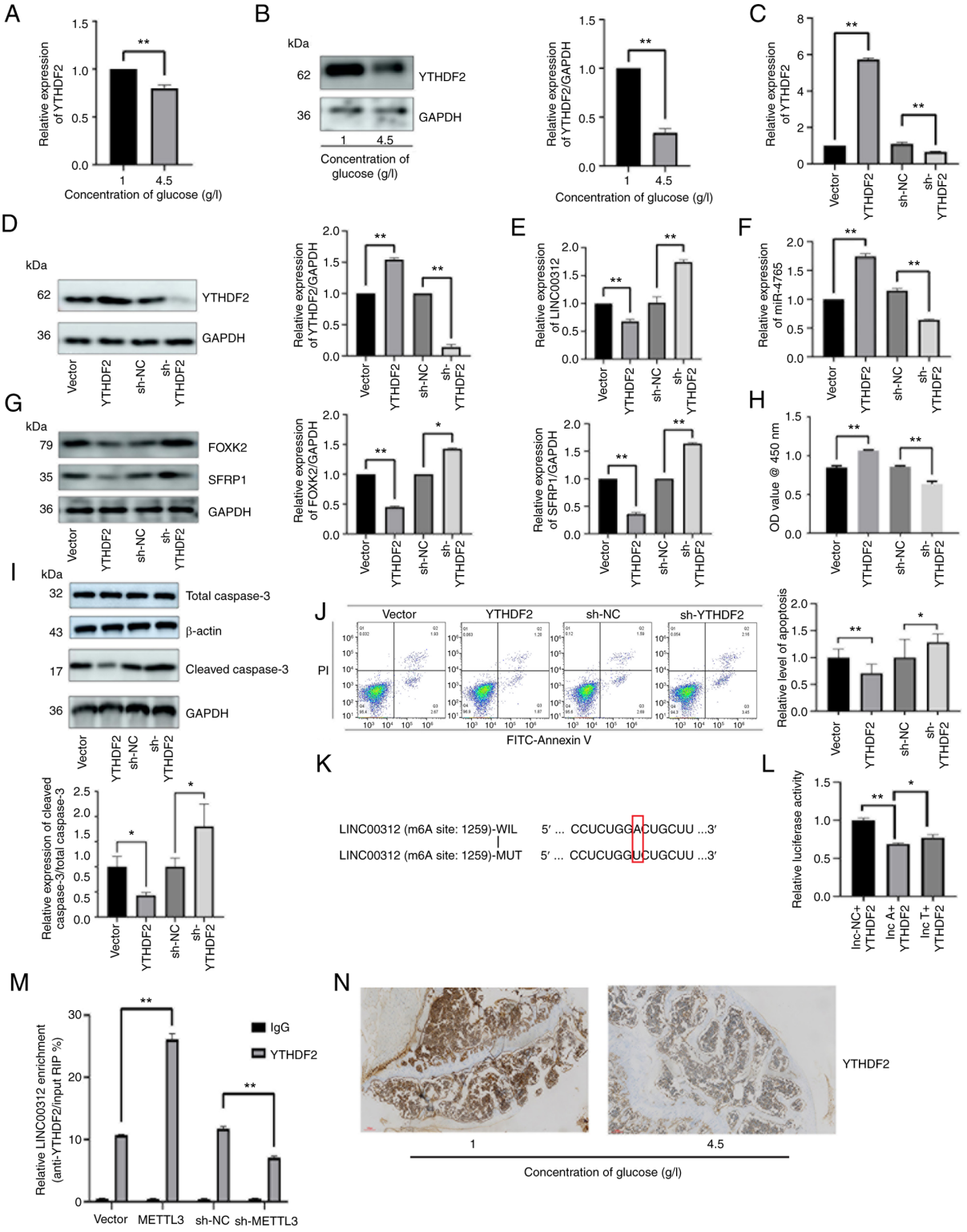

Figure 9. YTHDF2 participates in increasing the methylation level of LINC00312. (A) YTHDF2 mRNA expression in hFOB 1.19 cells under various glucose concentrations (1 or 4.5 g/l). (B) YTHDF2 protein expression in hFOB 1.19 cells under various glucose concentrations (1 or 4.5 g/l). (C) Transfection efficiency of YTHDF2 OE plasmids and sh-YTHDF2. YTHDF2 mRNA expression after transfection with YTHDF2 OE plasmids, sh-YTHDF2, and the corresponding NCs. (D) Transfection efficiency of YTHDF2 OE plasmids and sh-YTHDF2. YTHDF2 protein expression after transfection with YTHDF2 OE plasmids, sh-YTHDF2, and the corresponding NCs. (E) LINC00312 expression after transfection with YTHDF2 OE plasmids, sh-YTHDF2 and the corresponding NCs. (F) miR-4765 expression after transfection with YTHDF2 OE plasmids, sh-YTHDF2, and the corresponding NCs. (G) FOXK2 and SFRP1 protein expression after transfection with YTHDF2 OE plasmids, sh-YTHDF2, and the corresponding NCs. (H) Viability of hFOB 1.19 cells after transfection with YTHDF2 OE plasmids, sh-YTHDF2, and the corresponding NCs. Cell viability was expressed as OD values. (I) Cleaved caspase-3 protein expression after transfection with YTHDF2 OE plasmids, sh-YTHDF2, and the corresponding NCs. (J) Apoptosis level determined via Annexin V staining after transfection with YTHDF2 OE plasmids, sh-YTHDF2, and the corresponding NCs. (K) m6A modification locations of LINC00312. (L) Luciferase activity in 293T cells co-transfected with YTHDF2 OE plasmids and LINC00312 WT or MUT 3'-region. (M) Relative enrichment of YTHDF2 in LINC00312 after transfection with METTL3 OE plasmids, sh-METTL3, and the corresponding NCs. (N) YTHDF2 protein expression determined via immunohistochemical staining in the bone tissues of diabetic mice with osteoporosis and non-diabetic mice. Data are presented as the mean ± standard deviation (n=3). *P<0.05 and **P<0.01. WT, wild type; MUT, mutant; NC, negative control; OD, optical density; OE, overexpression; sh-, short hairpin; miR, microRNA.

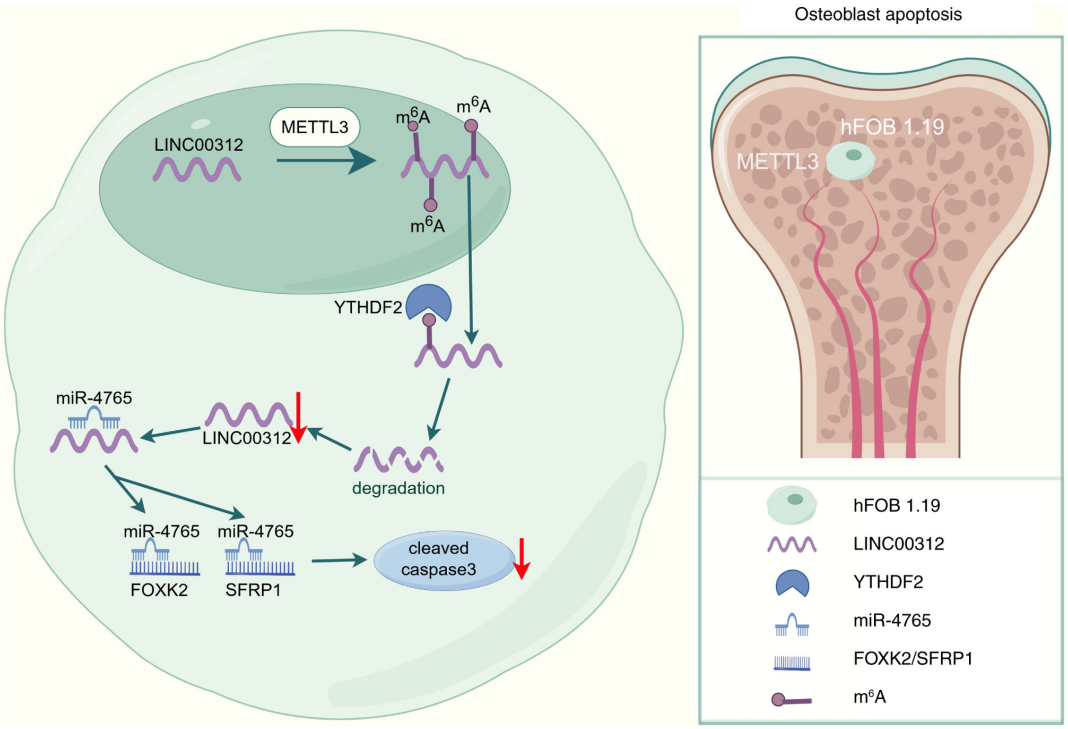

Figure 10. Graphic abstract. LINC00312 increases apoptosis of hFOB 1.19 cells by targeting the miR-4765-FOXK2/SFRP1 axis, which is m6A modified by METTL3 in a YTHDF2-dependent manner. miR, microRNA. The image was created using www.Figdraw.com.

consistent with the results presented herein. For example, a previous study found that LINC00312 enhances the sensitivity of the cisplatin-resistant ovarian cancer subline SKOV3/DDP to cisplatin by promoting apoptosis via the Bcl-2/Caspase-3 signaling pathway (42). Another study showed that forced expression of LINC00312 using a lentiviral vector inhibited proliferation and induced apoptosis in human hepatoblastoma and primary human hepatocellular carcinoma cells (43). LINC00312, which is regulated by HOXA5, has also been found to inhibit tumor proliferation and promote apoptosis in non-small cell lung cancer (44). Additionally, LINC00312 inhibits the proliferation of nasopharyngeal carcinoma cells and induces apoptosis (45).

Previous studies have demonstrated that METTL3 inhibits OP. METTL3 expression is upregulated during osteogenic differentiation of BMSCs (46). A previous study using osteoporotic models showed that METTL3 expression levels were reduced and that METTL3 silencing inhibited the osteogenic differentiation of BMSCs (47) and adipose-derived stem cells (48), ultimately leading to OP in mice (49). METTL3 has also been reported to alleviate OP by promoting osteogenic differentiation through the Wnt signaling pathway (50), LINC00657/miR-144-3p/BMPR1B axis (51), and MIR99AHG/miR-4660 axis (52). Moreover, Chinese *Ecliptae* herba has been found to possess therapeutic effects against OP by increasing METTL3 expression (53). One study indicated that METTL3 can trigger the development of OP. Another study using mouse calvaria-derived 3T3-like established 1 cells demonstrated that a METTL3 knockout could treat OP by reducing ferroptosis levels (54). Other studies have shown that METTL3 facilitates OP by promoting osteoclast differentiation (55).

Interestingly, three potential conflict points can be established: First, the different cell types involved, with osteogenesis acting on mesenchymal stem cells or osteoblasts, while osteoclastogenesis targets monocyte precursors; second, different molecular levels of action, with osteogenesis regulating mRNA stability (for example, embryonic lethal, abnormal vision, Drosophila-like 1 target) and miRNA processing (56,57), whereas osteoclastogenesis operates through the ceRNA mechanism (58); and the third and most critical point, the complete independence of downstream pathways, with osteogenesis following the Wnt/β-catenin or BMP pathways, and osteoclastogenesis relying on RANK/RANKL signaling. This tissue-specific regulation is akin to the same key (METTL3), which allows different locks (cell environments) to access different doors (pathways). Given that bone homeostasis relies on the balance between osteogenesis and osteoclastogenesis, the dual role of METTL3 may represent a natural mechanism for maintaining equilibrium, similar to controlling the accelerator and brake. However, under pathological conditions (for example, diabetes or postmenopausal estrogen deficiency), changes in the microenvironment induce an imbalance.

As a therapeutic target, METTL3 regulates the maturation of miR-324-5p and miR-4526, activates the osteogenic pathway (56,57), and blocks the methylation of circ_0008542, thereby inhibiting the bidirectional effects of the osteoclastic pathway on bone metabolism (58); however, its use requires cell type-specific regulation to avoid conflicting bidirectional effects. Although METTL3 expression is directly associated with bone metabolic activity, clinically validated data are still lacking (59). Regarding the synergistic effect, METTL3 agonists could theoretically promote osteogenesis while

bisphosphonates inhibit bone resorption, leading to complementary therapeutic benefits. Animal experiments have shown that miR-324-5p promotes significant bone regeneration, suggesting synergistic enhancement (56). However, the current findings remain at the mechanistic and theoretical levels, and direct evidence from clinical research is yet to be obtained.

YTHDF2 targets ncRNAs to release their osteogenic potential. For example, YTHDF2 has been shown to promote bone formation by degrading the inhibitory lncRNA LINC01013, thereby relieving the suppression of osteogenic genes (for example, osteocalcin and bone sialoprotein) (60). This mechanism is similar to our hypothesis in the current study, in which the degradation of LINC00312 promotes bone formation. Both mechanisms suggest the enhancement of osteogenesis through the clearance of inhibitory factors, with differences in their biological outcomes. A previous study emphasized the promotion of osteogenic differentiation, whereas the current study highlighted the inhibition of osteogenic apoptosis. Although existing literature has only reported LINC01013 as a target of YTHDF2, the current study, to the best of the authors' knowledge, is the first to reveal the inhibitory effects of LINC00312, thereby expanding the target spectrum of YTHDF2. The differences from previous findings are mainly attributable to the type of target gene, which ultimately determines the functional direction. First, targeting promoting factors inhibits bone formation; that is, YTHDF2 significantly inhibits osteoblast differentiation and mineralization by degrading runt-related transcription factor 2 mRNA (61). Similarly, YTHDF2 binds to fibroblast growth factor 21 mRNA (a factor that promotes bone formation), which may indirectly inhibit osteogenic differentiation under hyperglycemic conditions by mediating its degradation (62). Second, the present study focused on the regulation of cell fate rather than on direct osteogenesis. In this context, YTHDF2 inhibits bone resorption by degrading osteoclast-related genes (for example, Traf6 and Map4k4) and suppressing the NF-κB/MAPK pathway (63,64).

The present study has some notable limitations. Although the role of LINC00312 and FOXK2/SFRP1 in hFOB 1.19 cells was directly investigated, their levels in healthy individuals and patients with OP remain unclear. However, further studies are required to explore the clinical relevance of LINC00312 and FOXK2/SFRP1 expression. The present study primarily examined osteoblast apoptosis in OP; however, it did not provide a systematic analysis of osteogenic differentiation, such as the expression of specific differentiation markers or mineralization dynamics. Future studies could include the time-course detection of key markers, such as Runx2 and ALP, as well as the assessment of mineralized nodule formation. Additionally, *in vivo* double-fluorescence labeling can be used to quantify the dynamic mineral deposition rates. These approaches would help clarify the overall impact of the intervention on osteogenic function, thereby offering a more comprehensive understanding of bone formation mechanisms and supporting the development of optimized targeted therapies.

In conclusion, the findings of the present study demonstrated that LINC00312 promotes the apoptosis of hFOB 1.19 cells by targeting the miR-4765-FOXK2/SFRP1 axis. Moreover, miR-4765 OE downregulated FOXK2/SFRP1 expression and decreased apoptosis of hFOB 1.19 cells. Collectively, these findings indicated that the LINC00312/miR-4765/FOXK2/SFRP1 axis, which is m6A modified by METTL3 in a YTHDF2-dependent manner, may be a novel biomarker and therapeutic target for OP (Fig. 10).

Acknowledgements

Not applicable.

Funding

No funding was received.

Availability of data and materials

The data generated in the present study may be requested from the corresponding author.

Authors' contributions

YW conceived and designed the present study. YT performed the language editing, arrangement of data and drawing of figures. GY performed bioinformatics analysis. All authors read and approved the final version of this manuscript. YW, YT and GY confirm the authenticity of all the raw data.

Ethics approval and consent to participate

All animal experiments were performed in accordance with the National Institutes of Health Guide for the Care and Use of Laboratory Animals and were approved by the Institutional Review Board of the General Hospital of the Northern Theater Command (approval no. 2025-26; Shenyang, China).

Patient consent for publication

Not applicable.

Competing interests

The authors declare that they have no competing interests.

References

1. Hendrickx G, Boudin E and Van Hul W: A look behind the scenes: The risk and pathogenesis of primary osteoporosis. Nat Rev Rheumatol 11: 462-474, 2015.
2. US Preventive Services Task Force; Grossman DC, Curry SJ, Owens DK, Barry MJ, Caughey AB, Davidson KW, Doubeni CA, Epling JW Jr, Kemper AR, *et al*: Vitamin D, calcium, or combined supplementation for the primary prevention of fractures in community-dwelling adults: US preventive services task force recommendation statement. JAMA 319: 1592-1599, 2018.
3. Kern LM, Powe NR, Levine MA, Fitzpatrick AL, Harris TB, Robbins J and Fried LP: Association between screening for osteoporosis and the incidence of hip fracture. Ann Intern Med 142: 173-181, 2005.
4. Chotiyarnwong P and McCloskey EV: Pathogenesis of glucocorticoid-induced osteoporosis and options for treatment. Nat Rev Endocrinol 16: 437-447, 2020.
5. Ambrogini E, Almeida M, Martin-Millan M, Paik JH, Depinho RA, Han L, Goellner J, Weinstein RS, Jilka RL, O'Brien CA and Manolagas SC: FoxO-mediated defense against oxidative stress in osteoblasts is indispensable for skeletal homeostasis in mice. Cell Metab 11: 136-146, 2010.

6. Wu M, Ai W, Chen L, Zhao S and Liu E: Bradykinin receptors and EphB2/EphrinB2 pathway in response to high glucose-induced osteoblast dysfunction and hyperglycemia-induced bone deterioration in mice. Int J Mol Med 37: 565-574, 2016.
7. Wongdee K and Charoenphandhu N: Update on type 2 diabetes-related osteoporosis. World J Diabetes 6: 673-678, 2015.
8. Kushwaha P, Ahmad N, Dhar YV, Verma A, Haldar S, Mulani FA, Trivedi PK, Mishra PR, Thulasiram HV and Trivedi R: Estrogen receptor activation in response to Azadirachtin A stimulates osteoblast differentiation and bone formation in mice. J Cell Physiol 234: 23719-23735, 2019.
9. Tyagi AM, Mansoori MN, Srivastava K, Khan MP, Kureel J, Dixit M, Shukla P, Trivedi R, Chattopadhyay N and Singh D: Enhanced immunoprotective effects by anti-IL-17 antibody translates to improved skeletal parameters under estrogen deficiency compared with anti-RANKL and anti-TNF-α antibodies. J Bone Miner Res 29: 1981-1992, 2014.
10. Tamura Y, Kawao N, Yano M, Okada K, Okumoto K, Chiba Y, Matsuo O and Kaji H: Role of plasminogen activator inhibitor-1 in glucocorticoid-induced diabetes and osteopenia in mice. Diabetes 64: 2194-2206, 2015.
11. Rojas E, Carlini RG, Clesca P, Arminio A, Suniaga O, De Elguezabal K, Weisinger JR, Hruska KA and Bellorin-Font E: The pathogenesis of osteodystrophy after renal transplantation as detected by early alterations in bone remodeling. Kidney Int 63: 1915-1923, 2003.
12. Zhang H, Wang Y and He Z: Glycine-histidine-lysine (GHK) alleviates neuronal apoptosis due to intracerebral hemorrhage via the miR-339-5p/VEGFA pathway. Front Neurosci 12: 644, 2018.
13. Xu X, Yang J, Ye Y, Chen G, Zhang Y, Wu H, Song Y, Feng M, Feng X, Chen X, *et al*: SPTBN1 prevents primary osteoporosis by modulating osteoblasts proliferation and differentiation and blood vessels formation in bone. Front Cell Dev Biol 9: 653724, 2021.
14. Zhang Y, Cao X, Li P, Fan Y, Zhang L, Li W and Liu Y: PSMC6 promotes osteoblast apoptosis through inhibiting PI3K/AKT signaling pathway activation in ovariectomy-induced osteoporosis mouse model. J Cell Physiol 235: 5511-5524, 2020.
15. Glasner H, Riml C, Micura R and Breuker K: Label-free, direct localization and relative quantitation of the RNA nucleobase methylations m6A, m5C, m3U, and m5U by top-down mass spectrometry. Nucleic Acids Res 45: 8014-8025, 2017.
16. Kang HJ, Cheon NY, Park H, Jeong GW, Ye BJ, Yoo EJ, Lee JH, Hur JH, Lee EA, Kim H, *et al*: TonEBP recognizes R-loops and initiates m6A RNA methylation for R-loop resolution. Nucleic Acids Res 49: 269-284, 2021.
17. Blanco S, Bandiera R, Popis M, Hussain S, Lombard P, Aleksic J, Sajini A, Tanna H, Cortés-Garrido R, Gkatza N, *et al*: Stem cell function and stress response are controlled by protein synthesis. Nature 534: 335-340, 2016.
18. Shen W, Gao C, Cueto R, Liu L, Fu H, Shao Y, Yang WY, Fang P, Choi ET, Wu Q, *et al*: Homocysteine-methionine cycle is a metabolic sensor system controlling methylation-regulated pathological signaling. Redox Biol 28: 101322, 2020.
19. Qin Y, Li L, Luo E, Hou J, Yan G, Wang D, Qiao Y and Tang C: Role of m6A RNA methylation in cardiovascular disease (Review). Int J Mol Med 46: 1958-1972, 2020.
20. Abelson S: Eureka-DMA: An easy-to-operate graphical user interface for fast comprehensive investigation and analysis of DNA microarray data. BMC Bioinformatics 15: 53, 2014.
21. Zhou X, Su Z, Sammons RD, Peng Y, Tranel PJ, Stewart CN Jr and Yuan JS: Novel software package for cross-platform transcriptome analysis (CPTRA). BMC Bioinformatics 10 (Suppl 11): S16, 2009.
22. De-Ugarte L, Yoskovitz G, Balcells S, Güerri-Fernández R, Martinez-Diaz S, Mellibovsky L, Urreizti R, Nogués X, Grinberg D, García-Giralt N and Díez-Pérez A: MiRNA profiling of whole trabecular bone: Identification of osteoporosis-related changes in MiRNAs in human hip bones. BMC Med Genomics 8: 75, 2015.
23. Sukonina V, Ma H, Zhang W, Bartesaghi S, Subhash S, Heglind M, Foyn H, Betz MJ, Nilsson D, Lidell ME, *et al*: FOXK1 and FOXK2 regulate aerobic glycolysis. Nature 566: 279-283, 2019.
24. Shan L, Zhou X, Liu X, Wang Y, Su D, Hou Y, Yu N, Yang C, Liu B, Gao J, *et al*: FOXK2 elicits massive transcription repression and suppresses the hypoxic response and breast cancer carcinogenesis. Cancer Cell 30: 708-722, 2016.
25. Bowman CJ, Ayer DE and Dynlacht BD: Foxk proteins repress the initiation of starvation-induced atrophy and autophagy programs. Nat Cell Biol 16: 1202-1214, 2014.
26. Zhang F, Ma X, Li H, Zhang Y, Li X, Chen L, Guo G, Gao Y, Gu L, Xie Y, *et al*: FOXK2 suppresses the malignant phenotype and induces apoptosis through inhibition of EGFR in clear-cell renal cell carcinoma. Int J Cancer 142: 2543-2557, 2018.
27. Marais A, Ji Z, Child ES, Krause E, Mann DJ and Sharrocks AD: Cell cycle-dependent regulation of the forkhead transcription factor FOXK2 by CDK·cyclin complexes. J Biol Chem 285: 35728-35739, 2010.
28. Cui Z, Liu L, Kwame Amevor F, Zhu Q, Wang Y, Li D, Shu G, Tian Y and Zhao X: High expression of miR-204 in chicken atrophic ovaries promotes granulosa cell apoptosis and inhibits autophagy. Front Cell Dev Biol 8: 580072, 2020.
29. Esteve P, Rueda-Carrasco J, Inés Mateo M, Martin-Bermejo MJ, Draffin J, Pereyra G, Sandonís Á, Crespo I, Moreno I, Aso E, *et al*: Elevated levels of secreted-frizzled-related-protein 1 contribute to Alzheimer's disease pathogenesis. Nat Neurosci 22: 1258-1268, 2019.
30. Esteve P, Sandonìs A, Cardozo M, Malapeira J, Ibañez C, Crespo I, Marcos S, Gonzalez-Garcia S, Toribio ML, Arribas J, *et al*: SFRPs act as negative modulators of ADAM10 to regulate retinal neurogenesis. Nat Neurosci 14: 562-569, 2011.
31. Rodriguez J, Esteve P, Weinl C, Ruiz JM, Fermin Y, Trousse F, Dwivedy A, Holt C and Bovolenta P: SFRP1 regulates the growth of retinal ganglion cell axons through the Fz2 receptor. Nat Neurosci 8: 1301-1309, 2005.
32. Renström J, Istvanffy R, Gauthier K, Shimono A, Mages J, Jardon-Alvarez A, Kröger M, Schiemann M, Busch DH, Esposito I, *et al*: Secreted frizzled-related protein 1 extrinsically regulates cycling activity and maintenance of hematopoietic stem cells. Cell Stem Cell 5: 157-167, 2009.
33. Gu H, Shi S, Xiao F, Huang Z, Xu J, Chen G, Zhou K, Lu L and Yin X: MiR-1-3p regulates the differentiation of mesenchymal stem cells to prevent osteoporosis by targeting secreted frizzled-related protein 1. Bone 137: 115444, 2020.
34. Tang L, Lu W, Huang J, Tang X, Zhang H and Liu S: miR-144 promotes the proliferation and differentiation of bone mesenchymal stem cells by downregulating the expression of SFRP1. Mol Med Rep 20: 270-280, 2019.
35. Gu H, Wu L, Chen H, Huang Z, Xu J, Zhou K, Zhang Y, Chen J, Xia J and Yin X: Identification of differentially expressed microRNAs in the bone marrow of osteoporosis patients. Am J Transl Res 11: 2940-2954, 2019.
36. Zhang X, Zhu Y, Zhang C, Liu J, Sun T, Li D, Na Q, Xian CJ, Wang L and Teng Z: miR-542-3p prevents ovariectomy-induced osteoporosis in rats via targeting SFRP1. J Cell Physiol 233: 6798-6806, 2018.
37. Liu HP, Hao DJ, Wang XD, Hu HM, Li YB and Dong XH: MiR-30a-3p promotes ovariectomy-induced osteoporosis in rats via targeting SFRP1. Eur Rev Med Pharmacol Sci 23: 9754-9760, 2019.
38. Guo Z, Wang YH, Xu H, Yuan CS, Zhou HH, Huang WH, Wang H and Zhang W: LncRNA linc00312 suppresses radiotherapy resistance by targeting DNA-PKcs and impairing DNA damage repair in nasopharyngeal carcinoma. Cell Death Dis 12: 69, 2021.
39. No authors listed: Expression of concern: Overexpression of long intergenic noncoding RNA LINC00312 inhibits the invasion and migration of thyroid cancer cells by down-regulating microRNA-197-3p. Biosci Rep 40: BSR-20170109_EOC, 2020.
40. Peng Z, Wang J, Shan B, Li B, Peng W, Dong Y, Shi W, Zhao W, He D, Duan M, *et al*: The long noncoding RNA LINC00312 induces lung adenocarcinoma migration and vasculogenic mimicry through directly binding YBX1. Mol Cancer 17: 167, 2018.
41. No authors listed: Retraction: Overexpression of long intergenic noncoding RNA LINC00312 inhibits the invasion and migration of thyroid cancer cells by down-regulating microRNA-197-3p. Biosci Rep 41: BSR-20170109_RET, 2021.
42. Zhang C, Wang M, Shi C, Shi F and Pei C: Long non-coding RNA Linc00312 modulates the sensitivity of ovarian cancer to cisplatin via the Bcl-2/Caspase-3 signaling pathway. Biosci Trends 12: 309-316, 2018.
43. Wu J, Zhou X, Fan Y, Cheng X, Lu B and Chen Z: Long non-coding RNA 00312 downregulates cyclin B1 and inhibits hepatocellular carcinoma cell proliferation in vitro and in vivo. Biochem Biophys Res Commun 497: 173-180, 2018.
44. Zhu Q, Lv T, Wu Y, Shi X, Liu H and Song Y: Long non-coding RNA 00312 regulated by HOXA5 inhibits tumour proliferation and promotes apoptosis in non-small cell lung cancer. J Cell Mol Med 21: 2184-2198, 2017.

45. Zhang W, Huang C, Gong Z, Zhao Y, Tang K, Li X, Fan S, Shi L, Li X, Zhang P, *et al*: Expression of LINC00312, a long intergenic non-coding RNA, is negatively correlated with tumor size but positively correlated with lymph node metastasis in nasopharyngeal carcinoma. J Mol Histol 44: 545-554, 2013.
46. Liu J, Chen M, Ma L, Dang X and Du G: piRNA-36741 regulates BMP2-mediated osteoblast differentiation via METTL3 controlled m6A modification. Aging (Albany NY) 13: 23361-23375, 2021.
47. Yan G, Yuan Y, He M, Gong R, Lei H, Zhou H, Wang W, Du W, Ma T, Liu S, *et al*: m^{6}A methylation of precursor-miR-320/RUNX2 controls osteogenic potential of bone marrow-derived mesenchymal stem cells. Mol Ther Nucleic Acids 19: 421-436, 2020.
48. Luo D, Peng S, Li Q, Rao P, Tao G, Wang L and Xiao J: Methyltransferase-like 3 modulates osteogenic differentiation of adipose-derived stem cells in osteoporotic rats. J Gene Med 25: e3481, 2023.
49. Wu Y, Xie L, Wang M, Xiong Q, Guo Y, Liang Y, Li J, Sheng R, Deng P, Wang Y, *et al*: Mettl3-mediated m^{6}A RNA methylation regulates the fate of bone marrow mesenchymal stem cells and osteoporosis. Nat Commun 9: 4772, 2018.
50. Wu T, Tang H, Yang J, Yao Z, Bai L, Xie Y, Li Q and Xiao J: METTL3-m^6 A methylase regulates the osteogenic potential of bone marrow mesenchymal stem cells in osteoporotic rats via the Wnt signalling pathway. Cell Prolif 55: e13234, 2022.
51. Peng J, Zhan Y and Zong Y: METTL3-mediated LINC00657 promotes osteogenic differentiation of mesenchymal stem cells via miR-144-3p/BMPR1B axis. Cell Tissue Res 388: 301-312, 2022.
52. Li L, Wang B, Zhou X, Ding H, Sun C, Wang Y, Zhang F and Zhao J: METTL3-mediated long non-coding RNA MIR99AHG methylation targets miR-4660 to promote bone marrow mesenchymal stem cell osteogenic differentiation. Cell Cycle 22: 476-493, 2023.
53. Tian S, Li YL, Wang J, Dong RC, Wei J, Ma Y and Liu YQ: Chinese ecliptae herba [Eclipta prostrata (L.) L.] extract and its component wedelolactone enhances osteoblastogenesis of bone marrow mesenchymal stem cells via targeting METTL3-mediated m6A RNA methylation. J Ethnopharmacol 312: 116433, 2023.
54. Lin Y, Shen X, Ke Y, Lan C, Chen X, Liang B, Zhang Y and Yan S: Activation of osteoblast ferroptosis via the METTL3/ASK1-p38 signaling pathway in high glucose and high fat (HGHF)-induced diabetic bone loss. FASEB J 36: e22147, 2022.
55. Wang C, Zhang X, Chen R, Zhu X and Lian N: EGR1 mediates METTL3/m^{6}A/CHI3L1 to promote osteoclastogenesis in osteoporosis. Genomics 115: 110696, 2023.
56. Xiao J, Xu Z, Deng Z, Xie J and Qiu Y: METTL3 facilitates osteoblast differentiation and bone regeneration via m6A-dependent maturation of pri-miR-324-5p. Cell Immunol 413: 104974, 2025.
57. Song Y, Gao H, Pan Y, Gu Y, Sun W and Liu J: METTL3 promotes osteogenesis by regulating N6-methyladenosine-dependent primary processing of hsa-miR-4526. Stem Cells 43: sxae089, 2025.
58. Wang W, Qiao SC, Wu XB, Sun B, Yang JG, Li X, Zhang X, Qian SJ, Gu YX and Lai HC: Circ_0008542 in osteoblast exosomes promotes osteoclast-induced bone resorption through m6A methylation. Cell Death Dis 12: 628, 2021.
59. Liu J, Chen X and Yu X: Unraveling the role of N6-methylation modification: From bone biology to osteoporosis. Int J Med Sci 22: 2545-2559, 2025.
60. Song J, Wang Y, Zhu Z, Wang W, Yang H and Shan Z: Negative regulation of LINC01013 by METTL3 and YTHDF2 enhances the osteogenic differentiation of senescent pre-osteoblast cells induced by hydrogen peroxide. Adv Biol (Weinh) 8: e2300642, 2024.
61. Sun Q, Zhao T, Li B, Li M, Luo P, Zhang C, Chen G, Cao Z, Li Y, Du M and He H: FTO/RUNX2 signaling axis promotes cementoblast differentiation under normal and inflammatory condition. Biochim Biophys Acta Mol Cell Res 1869: 119358, 2022.
62. Wang Z, Tang Y, Liu Y, Zeng Y and Zhang M: ALKBH5 mediates FGF21 m6A demethylation in human bone marrow mesenchymal stem cells under high glucose conditions. Biochem Biophys Res Commun 774: 152042, 2025.
63. Fang C, He M, Li D and Xu Q: YTHDF2 mediates LPS-induced osteoclastogenesis and inflammatory response via the NF-κB and MAPK signaling pathways. Cell Signal 85: 110060, 2021.
64. He J, Zhao Y, Zhang Y, Zhang Z, Li D and Xu Q: FTO regulates osteoclast development by modulating the proliferation and apoptosis of osteoclast precursors in inflammatory conditions. Cell Signal 117: 111098, 2024.